MATHEMATICAL MODELING OF VIRUS DYNAMICS IN IMMUNOLOGY

by

BARIS HANCIOGLU

B.S. in Mathematics, Bilkent University, Turkey, 1998

Laurea in Mathematics, Universita degli Studi di Milano, Italy, 2002

Submitted to the Graduate Faculty of

Arts and Sciences in partial fulfillment

of the requirements for the degree of

Doctor of Philosophy

University of Pittsburgh

2007

UNIVERSITY OF PITTSBURGH

FACULTY OF ARTS AND SCIENCES

This dissertation was presented

by

Baris Hancioglu

It was defended on

August 28, 2007

and approved by

Gilles Clermont, Prof., Critical Care Medicine

Bard Ermentrout, Prof., Mathematics

Jonathan Rubin, Prof., Mathematics

Shlomo Ta'asan, Prof. Mathematics

Sven Zenker, M.D., Critical Care Medicine

Committee Chair Person: David Swigon, Prof., Mathematics

MATHEMATICAL MODELING OF VIRUS DYNAMICS IN IMMUNOLOGY

Baris Hancioglu, Ph.D.

University of Pittsburgh, 2007

A simplified dynamical model of immune response to uncomplicated influenza virus infection is presented, which focuses on the control of the infection by the innate and adaptive immunity. Innate immunity is represented by interferon-induced resistance to infection of respiratory epithelial cells and by removal of infected cells by effector cells. Adaptive immunity is represented by virus-specific antibodies. Similar in spirit to the recent model of Bocharov & Romanyukha (Bocharov and Romanyukha, 1994), the model is constructed as a system of 10 ordinary differential equations with 27 parameters.

In the first part, parameter values for the model are obtained either from published experimental data or by estimation based on fitting available data about the time course of IAV infection in a naïve host. Sensitivity analysis is performed on the model parameters. To account for the variability and speed of adaptation, a variable is introduced that quantifies the antigenic compatibility between the virus and the antibodies. It is found that for small initial viral load the disease progresses through an asymptomatic course, for intermediate value it takes a typical course with constant duration and severity of infection but variable onset, and for large initial viral load the disease becomes severe. The absence of antibody response leads to recurrence of disease and appearance of a chronic state with nontrivial constant viral load.

In the second part, an ensemble model of immune response is developed, which consists of multiple ODE models that are identical in form but differ in parameter values. A probabilistic measure of goodness of fit of the ODE model is used to derive an a posteriori probability density

on the space of parameter values. This probability density is sampled using the Metropolis Monte Carlo method and sampling is enhanced using parallel tempering algorithm. The ensemble model is employed to compute probabilistic estimates on trajectory of the immune response, duration of disease, maximum damage, likelihood of rebound in the disease and the probability of occurrence of superspreaders. The effectiveness of using antiviral drug to treat the infection is addressed and optimal treatment scenarios are discussed.

To my wife, Sevim, and to my parents, Ilhan and Guzide, for their love and understanding

Acknowledgements

TABLE OF CONTENTS

LIST OF TABLES

LIST OF FIGURES

1.0   INTRODUCTION

Influenza is a highly cytopathic, contagious, acute respiratory disease caused by an influenza virus infection (Mohler et al., 2005; Nicholson K.G et al., 1998; Tamura et al., 2004). Transmission is caused by direct contact such as hand shake or by airborne virus (Mohler et al., 2005). The virus is an enveloped virus with seven internal proteins (nucleoprotein (NP), three polymerase proteins (PA, PB1, and PB2), two matrix proteins (M1 and M2), and nonstructural proteins (NS2)) and two external glycoproteins, hemagglutinin (HA) and neuraminidase (NA) (Tamura et al., 2005). It is divided into types A, B, and C, according to the antigenic differences between nucleoprotein (NP) and matrix protein (M) (Tamura et al., 2005). Influenza A viruses are subdivided into subtypes such as H1N1, H16N9 etc. based on the antigenic signatures of the major surface proteins HA (16 subtypes differ by 30%) and NA (Webster et al., 2006). The viruses in each subtype regularly undergo gradual changes in genetic makeup through point mutations in the HA and NA molecules (antigenic drift) which cause local outbreaks of influenza and small size epidemics. Occasionally, a major change in the HA and NA proteins can arise from the exchange of genetic material (reassortment) between the avian influenza gene pool and human influenza genes during co-infection (Tamura et al., 2004) or adaptive mutation. Such a change is termed as "antigenic shift" and since the population has typically limited or no immunity against the modified virus, a global pandemic may result.

In the 20th century, three global pandemics occurred. The "Spanish flu" of 1918-19, which was of the subtype H1N1, infected approximately one third of the entire human population(Taubenberger et al., 2006). More than a half million people died in the U.S. and about 50 million people died worldwide(Taubenberger et al., 2006). In 1957-58, "Asian flu" of the subtype H2N2 caused about 70,000 deaths in the U.S. In 1968-69, "Hong Kong flu" of the subtype H3N2 caused about 34,000 deaths in the U.S. Many scientists believe that it is only a matter of time until the next pandemic occurs. In the absence of proper preparation, a pandemic could cause 89,000 to 207,000 deaths, 314,000 to 734,000 hospitalizations, 18 to 42 million outpatient visits, and another 20 to 47 million people being sick in the U.S (Meltzer et al., 1999). The economic impact could range between $71.3 and $166.5 billion and between 15% and 35% of the U.S. population could be affected from the infection(Meltzer et al., 1999). Currently, there is a big concern about the pandemic potential of the avian flu of subtype H5N1 which has already caused considerable damage, mainly to birds: more than 140 million domestic birds have been killed by the virus or culled to stem its spread till now and more than 130 people have been infected in various countries in Asia(Webster et al., 2006). Almost half of the infected people died. These numbers show the potential danger of IAV infection for human population and the importance of understanding virus-immune system interactions which helps for taking necessary control measures (vaccination or antiviral drugs).

Mathematical modeling has proven to be a valuable tool in the understanding of immune response to infectious diseases (Perelson, 2002) which helps in clarifying and testing hypotheses, finding the smallest number of factors sufficient to explain the biological phenomena and analyzing experimental results(Asquith et al., 2003). Modeling has a substantial impact on research at the molecular level(Nowak et al., 2000). Recently, important results have been

obtained in the mathematical modeling of virus dynamics for the HIV (Nowak et al., 1996; Perelson et al., 1993; Perelson et al., 1996), hepatitis B(Marchuk et al., 1991), hepatitis C (Neumann et al., 1998)and influenza(Bocharov et al., 1994) infections.

This thesis is concerned with the development of a mathematical model of the dynamics of IAV infection and the human immune response to such infection. Two closely related types of models are discussed: a deterministic ODE model, which is derived and analyzed in the first part, and an ensemble model base on the ODE model that is discussed in the second part.

2.0   A DYNAMICAL MODEL OF HUMAN IMMUNE RESPONSE TO INFLUENZA VIRUS INFECTION

2.1   INTRODUCTION

In this part we construct a simplified, biologically justified, mathematical model of the dynamics of IAV infection and the human immune response to such infection. We do not strive to obtain a detailed model accounting for all known components of the immune system and their interactions. Rather, we focus on three important components of the immune response; the interferon and cellular components of innate immunity and the adaptive immunity. All of them have the same goal of limiting the concentration of the virus and the damage to the system. They achieve this goal using different strategies: interferon immunity by removing the "substrate" that virus needs for reproduction (i.e., the healthy cells), cellular immunity by removing the source of new viruses (i.e., the infected cells), and adaptive immunity by lowering the effective concentration of the virus.

Our main goal is to uncover the relative roles played by each immune strategy during the course of the disease to have a better understanding of what drives the intensity of symptoms, infectivity of the virus and the host and duration of the disease. In subsequent research, the model will serve as a tool for predicting the effect of therapeutic interventions on the course of the disease, as well as a model for understanding of basic processes of the immune response to

multiple infections. Our second goal is to develop a model of the immune response of individuals that can be used as a practical basis for multi-scale population susceptible-infected-recovered (SIR) models that are used to describe geographic disease spread and evaluate the impact of containment strategies. As such, this biological model should account for individual characteristics of the human host and the virulence of a specific virus subtype or strain and should yield predictions about the onset, severity and infectivity of the IAV infection in an individual as a function of the initial viral load and existing immunity(Clermont et al., 2004). Yet, the model should be sufficiently simple to allow fast computation of individual immune responses as part of multi-scale simulations.

2.2   BIOLOGICAL MODEL

Influenza virus (IAV) attacks the host respiratory tract mucosa, interacts with healthy epithelial cells and infects them by binding to cell surface receptors via one of the major surface glycoproteins, HA (Tamura et al., 2004). The virus replicates in infected cells and several hours after cellular infection, newly synthesized virus particles are released by the action of another major glycoprotein, NA (Tamura et al., 2005). The response of the host to IAV infection involves a cascade of events mediated by several effector cells and molecules (Ada et al., 1986; Tamura et al., 2004) that neutralize free virus, kill infected cells and limit the spread of viral particles by increasing healthy cell resistance to infection.

Antigen presenting cells (APC) are essential in the induction and amplification of the human immune response (Akira et al., 2001). Exogenous viral antigens, which comprise inactive viral particles, intact viruses and apoptotic, infected cells, are taken up by APC through

endocytosis and provide a potential source of peptides that could bind to MHC class I or II molecules in the APC (Nguyen et al., 1998; Tamura et al., 2004; Tulp et al., 1994). The role of the APC is to stimulate both innate and adaptive immunity.

As the first line of defense, APC and infected cells stimulate the innate immunity by secreting interferon α and β (IFN) molecules (Julkunen et al., 2000; Lamb R, 1996; Ronni et al., 1995; Sareneva et al., 1998), (Stark et al., 1998) which interact with healthy cells and convert them to an infection resistant state, thereby preventing the virus from spreading efficiently and allowing the adaptive immune response enough time to develop and eliminate the virus (Price et al., 2000). Another role of IFN is to stimulate symptoms such as fever which occurs in the early stages of infection. IFN levels rise rapidly after infection and correlate directly with the degree of viral replication in ferrets, mice and humans (Tamura et al., 2004; Wyde et al., 1982). The magnitude of fever correlates strongly with the level of virus shedding in humans and animals (Tamura et al., 2004).

As a second line of defense, APC stimulate the cellular component of innate immunity which consists of effector cells (cytotoxic T cells (CTL) or natural killer cells (NK)) that destroy infected cells before they can release a mature virus. Activated T cells produce various factors which are extremely important for the kinetics of the IAV infection: helper T cells secrete IL-2 and other lymphocytes and CTL produce IFN-γ, which increases the expression of MHC antigens acting to enhance virus-infected cell destruction. The peptide-class I MHC complexes presented on the infected cells are recognized by class-I MHC-restricted CD8^{+} memory T cells (Th1 cells), which destroy the infected cells (Tamura et al., 2005). The specificity of memory T cells is directed against viral internal proteins; NP is the strongest of these antigens (Yewdell et

al., 1985). Since structure of these antigens is conserved within the type of virus, Th1 cells against these antigens are cross-reactive within the type of influenza (Tamura et al., 2005).

Finally, APC stimulate adaptive immunity by activating the proliferation of virus-specific plasma cells which produce antibodies (Abs) that bind with IAV and render it ineffective. HA and NA are taken up in an endocytic vesicle pathway of the APC and are degraded; the peptides of these antigens are loaded on class-II MHC molecules and then expressed on the APC (Tulp et al., 1994).The peptide class II MHC complexes are recognized by class-II MHC-restricted CD4$^+$ T cells (Th2 cells). Th2 cell stimulation by antigen recognition results in the production of specific Abs to HA and NA molecules. Anti-HA Abs neutralize the infectivity of the virus, whereas anti-NA Abs prevent the release of viruses from infected cells (Johansson et al., 1989). Thus, anti-HA Abs are primarily responsible for preventing infection, while anti-NA Abs and CTL specific for viral core proteins are responsible for reducing viral spread and thereby for accelerating the recovery from influenza(Tamura et al., 2005).

The respiratory tract mucosa is not only the site of infection by influenza viruses but also the site of defense against viral infection in the host (Tamura et al., 2004). The recovery process after primary infection involves two phases: An early phase (days 5-7), characterized by a rapid decrease in virus titer via killing of the virus-infected epithelial cells by MHC class I restricted CD8$^+$ CTL's, which appear with a peak at day 7 is cellular response dependent, while a late phase (day 7 onwards), characterized by a more protracted decrease that ultimately results in clearance, depends on the adaptive response (Tamura et al., 2004). Since flu symptoms emerge within a few days of inoculation, acquired immunity appearing after the first week of infection cannot prevent the onset of respiratory symptoms. Therefore, effective immunity must be induced in advance by natural infection or vaccination in order to prevent disease.

2.3   MATHEMATICAL MODEL

The model of human immune response against IAV infection we consider is a simplified

model of population-dynamics type which consists of the following interactions (see Figure 2-1):

The epithelial cells of the respiratory tract are assumed to be in one of four possible states:

healthy (H), infected (I), dead (D), or resistant (R) to infection. The total number of epithelial

cells (i.e., $H + I + D + R$) is assumed constant. The virus particles (V) interact with healthy cells

and infect them. Infected cells release new virus particles upon their death. Proliferation of

healthy cells causes regeneration and decrease in the proportion of dead cells.   Dead cells

stimulate the activation of APC (M). APC stimulate the production of interferon α and β (F)
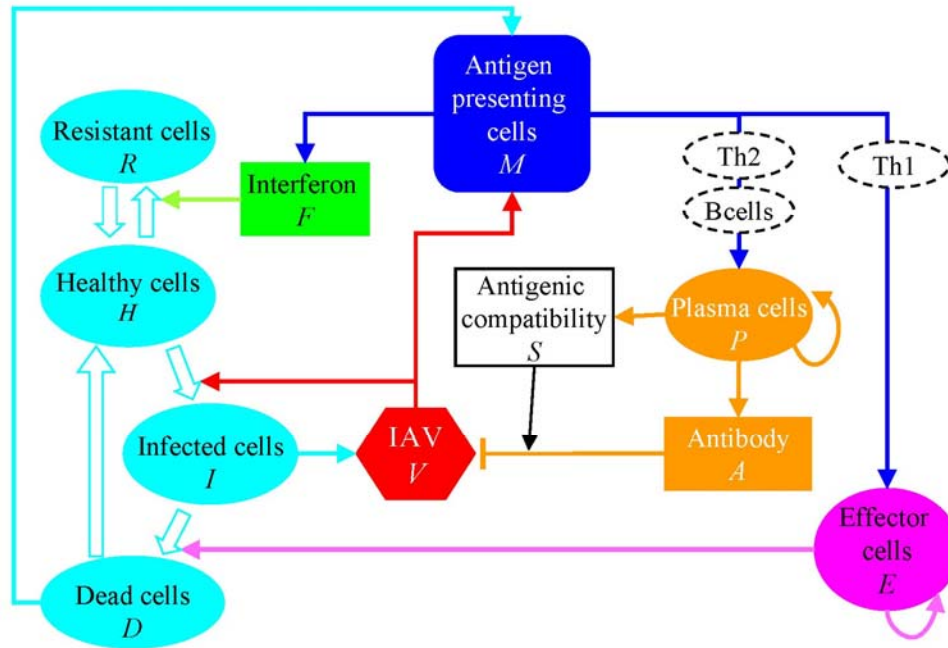
Figure 2-1. Schematic representation of interactions included in the model.

The influenza virus (IAV) is shown as red hexagon, the four different cell types are shown in cyan. Components of adaptive immunity are shown in orange, cellular component of innate immunity in purple, and interferon component in green. Upregulation is represented by lines terminated with arrows and inhibition by lines terminated with bars.

8

that interact with healthy cells and convert them to a resistant state. APC also stimulate the proliferation of effector cells (E) that destroy infected cells. Finally, they stimulate the production of plasma cells (P) which, in turn, produce antibodies (A) that neutralize (kills) virus. This neutralization is modulated by the antigenic compatibility (S) between virus and antibodies currently produced by the organism. S quantifies the affinity between antibodies and virus.

These interactions were used in the construction of a system of 10 ordinary differential equations describing the dynamics of the main variables, listed in Table 2-1, which correspond to the components of the immune response shown in Figure 2-1:

Table 2-1. Model variables and scaling factors.

Variable	Description	Scaling factor
V	Viral load per epithelial cell[*]	$H^* = 1.7 \times 10^{-11}$ M
H	Proportion of healthy cells	$H^* = 1.7 \times 10^{-11}$ M
I	Proportion of infected cells	$H^* = 1.7 \times 10^{-11}$ M
M	Activated antigen presenting cells per homeostatic level	$M^* = 10^{-15}$ M
F	Interferons per homeostatic level of macrophages	$M^* = 10^{-15}$ M
R	Proportion of resistant cells	$H^* = 1.7 \times 10^{-11}$ M
E	Effector cells per homeostatic level	$E^* = 10^{-16}$ M
P	Plasma cells per homeostatic level	$P^* = 1.8139 \times 10^{-20}$ M
A	Antibodies per homeostatic level	$A^* = 7.2 \times 10^{-11}$ M
S	Antigenic compatibility	

$$\frac{dV}{dt} = \gamma_V I - \gamma_{VA} SAV - \gamma_{VH} HV - \alpha_V V - \frac{a_{V1}V}{1 + a_{V2}V} \tag{1}$$

$$\frac{dH}{dt} = b_{HD} D(H + R) + a_R R - \gamma_{HV} VH - b_{HF} FH \tag{2}$$

$$\frac{dI}{dt} = \gamma_{HV} VH - b_{IE} EI - a_I I \tag{3}$$

$$\frac{dM}{dt} = (b_{MD} D + b_{MV} V)(1 - M) - a_M M \tag{4}$$

$$\frac{dF}{dt} = b_F M + c_F I - b_{FH} HF - a_F F \tag{5}$$

$$\frac{dR}{dt} = b_{HF} FH - a_R R \tag{6}$$

$$\frac{dE}{dt} = b_{EM} ME - b_{EI} IE + a_E(1 - E) \tag{7}$$

$$\frac{dP}{dt} = b_{PM} MP + a_P(1 - P) \tag{8}$$

$$\frac{dA}{dt} = b_A P - \gamma_{AV} SAV - a_A A \tag{9}$$

$$\frac{dS}{dt} = rP(1 - S) \tag{10}$$

No differential equation is needed for the proportion of dead cells (*D*) which is given by

$$D = 1 - H - R - I \tag{11}$$

The variable *D* serves as a marker for tissue damage (Hayden et al., 1998) and an indicator of the severity of disease. All variables have been rescaled by their constant homeostatic values (see Table 2-1) and hence the system (1)-(11) is dimensionless.

The interactions are based on clonal selection theory, mass-action kinetics, characteristics of interactions and the birth-death balances of populations of cells and molecules: Equation (1) of the system describes the rate of change of virus concentration *V*. It expresses the production rate of a viral particle by infected cells, rate of neutralization of IAV by specific antibodies, the rate of adsorption of viral particles by healthy cells, and the natural decay of viral particles. The viral particles are also removed from the respiratory tract by nonspecific mechanisms. The non-specific mucociliary removal of virions supported by cough and other mechanisms is described by the term $(a_{V1}V)/(1+a_{V2}V)$, which saturates with increasing *V* as the available capacity of these mechanisms is exhausted. Note that the lethal damage of an infected cell by the effector cells doesn't cause any release of infective IAV and hence in equation (1) there is no term of the form *EI*.

Equation (2) determines the time rate of change of healthy cells *H*. During recovery, new healthy cells are generated as a result of proliferation of both healthy and resistant cells (the offspring of resistant cells lose resistance) and hence the proliferation term is proportional to (*H+R*), and to *D* (in a logistic fashion) since regeneration can only occur in the presence of damage. Resistant cells *R* gradually loose their resistance to infection and return into their initial sensitive state (healthy state) (Joklik, 1985) , which is characterized by the term $a_R R$. The term $\gamma_{HV}VH$ is the loss of healthy cells due to infection and the term $b_{HF}FH$ characterizes transition of the healthy cells into resistant state.

Equation (3) characterizes the time rate of change of infected cells *I*. The infection of healthy cells by virions is described in the term $\gamma_{HV}VH$. The term $a_I I$ indicates the natural death of infected cells during which new virus particles are produced. The term $b_{IE}EI$ characterizes the

11

destruction of infected cells by effector cells (CTL and NK) during which no new virus is produced.

Equation (4) establishes that the time rate of increase of activated APC (M) is proportional to the amount of the virus and the amount of dead cells. The natural decay of activated state of APC is represented by the last term in that equation.

Equation (5) describes the time rate of change of interferons α and β (F) which depends on the production rate of F by APC and by infected cells, on the rate of F binding healthy cells, as well as on the non-specific decay of F.

Equation (6) shows that resistant cells R are induced from healthy cells ($b_{HF}FH$) and convert back to healthy cells (a_RR) with finite lifetime.

Equation (7) characterizes the rate of change of effector cells E concentration and takes into account the production rate of effector cells stimulated by APC (first term) and the destruction rate of infected cells by effector cells (second term, $b_{EI}IE$). The terms $a_E(1-E)$ and $a_P(1-P)$ in equations (7) and (8) are approximate expressions for homeostatic maintenance of the levels of active effectors and plasma cells, reflecting the observation that the healthy body tends to maintain their concentrations within narrow bounds. In a healthy state the effectors and plasma cells are naturally located in lymph nodes and blood, and migrate into the infected tissue upon activation. Both the activation and migration of those cells to the infected tissue are assumed to be much faster than their proliferation and hence are not explicitly accounted for. The first term in equation (8) characterizes the activation process of plasma cells stimulated by APC.

Equation (9) stands for the time rate of change of the concentration of antibodies A describing the production rate of A by plasma cells (first term), the neutralization rate of free viral particles by specific antibodies (second term) and the natural decay rate of A (last term).

The variable S in our model represents the compatibility between antibodies and the virus strain in an individual and ranges from 0 (no compatibility) to 1 (maximal compatibility) and can be interpreted as a measure of binding affinity of the antibody and the virus (Smith et al., 1999). The immune memory of the host is described by the initial value $S(0)$ of S. During the course of the disease, S increases as plasma cells produce antibodies increasingly compatible with viral antigens. The rate of increase of S is approximated by the term $rP(1-S)$ which accounts for two natural observations: (i) the increase in S is stimulated by plasma cells and (ii) S cannot increase beyond 1. By adjusting the time evolution of S we may observe how the course of the disease depends on the evolution of antigenic distance.

It has been established that IAV boosts T cell and B cell memory (Ada et al., 1986). However, the majority of IAV-induced CTL are fully cross-reactive with related strains and would provide heterotypic immunity, while antibodies (and consequently B memory cells) are protective only against reinfection by strains closely related to the stimulating IAV (Bocharov et al., 1994). Thus a variable analogous to S for description of the antigenic distance between effectors and the virus is not necessary.

We note that a number of assumptions in the model are strong simplifications of our knowledge of immune physiology. The populations of cells and virions are assumed to be uniformly distributed over the epithelial layer at all times. It is also assumed that time rate of change of any model variable is determined by the present value of all variables. Some of the variables do not have uniquely identifiable biological counterparts. For example, there is no single biological entity or marker that represents the APC in our model, which are assumed to provide both antigen presenting and IFN producing functions. We have also omitted intermediate steps in the pathways: for example, we do not account for the intermediate steps in the

production of effector cells and plasma cells such as Th1 and Th2 helper cells and B-cells. We do not consider time delays in the reproduction of cellular components.

Although our model is similar on that of Bocharov et al, (Bocharov et al., 1994) it differs in number of instances that reflect the latest knowledge about biology of influenza: (i) we include a new nonspecific virus removal term in Equation (1), which results in clearing out extremely low initial virus concentrations, (ii) we make the cell regeneration rate proportional to the product of healthy cells and dead cells, as opposed to only dead cells, (iii) we include reproduction of resistant cells, (iv) we make the activation of APC proportional to the amount of both viral particles and dead cells, (v) we include a new term describing the production of interferons by infected cells, (vi) we introduce a new variable that accounts for the antigenic distance between antibodies and the virus.

2.4   SIMULATIONS

We use the dynamical systems analysis software XPPAUT (www.pitt.edu/~phase/) to run all simulations. The time courses of variables were obtained by numerical integration using parameters provided in Table 2-2. Model parameters were adjusted so that the response of the naïve host to the standard initial conditions (see below) satisfies the following criteria, extracted from available experimental and clinical data (Bocharov et al., 1994): (i) Virus titers V peak 4-5 day after infection with an approximately 10^4 fold increase over the initial level. (ii) The maximum amount of activated APC M is 40%. APC become deactivated within 8-10 days. (iii) Effector cells E peak with approximately 10^2 fold increase over the homeostatic level. (iv) P cells peak with approximately 10^4 fold increase. (v) S changes gradually. After 15 days, the

antibodies *A* are compatible with the probability 0.8. (vi) Maximum level of dead cells D_{max} is 36%. (vii) Interferons *F* peak with approximately 10^4 fold increase. (viii) Antibodies *A* peak with approximately 10^3 fold increase. Most of our parameters are close to those in (Bocharov et al., 1994) yet rescaled to dimensionless quantities. To examine the robustness of infection dynamics to parameter values and to provide insight into inter-individual variation in disease dynamics, we conducted a full set of one-dimensional sensitivity analyses.

Table 2-2. Model parameters used for the baseline case

Parameter	Value	Description	Comments	Sources
γ_V	510	Rate constant of influenza A virus (IAV) particles secretion per infected epithelial cells	About 10^3-10^4 virus particles are released from a single infected cell within a day.	(Zdanov et al., 1969)
γ_{VA}	619.2	Rate constant of neutralization of IAV by antibodies	1-10 antibodies are sufficient to neutralize a single IAV (Wohlfart, 1988)	(Bocharov et al., 1994)
γ_{VH}	1.02	Rate constant of adsorption of IAV by infected epithelial cells	In vitro experiments show that a single epithelial cell can adsorb 1-10 influenza virions.	(Bocharov et al., 1994)
α_V	1.7	Rate constant of nonspecific IAV removal	Nonspecific physical removal of infective virions takes about 4-24 hours.	(Bocharov et al., 1994)
a_{V1}	100	Rate constant of nonspecific IAV removal		
a_{V2}	23000	Rate constant of nonspecific IAV removal		
b_{HD}	4	Rate constant of regeneration of epithelial cells	The duration of a single division of an epithelial cell is about 0.3-1 day.	(Keenan et al., 1982)
a_R	1	Rate constant of epithelial cells' virus resistance state decay		(Marchuk et al., 1991)
γ_{HV}	0.34	Rate constant of epithelial cells infected by IAV	The difference between γ_{VH} and γ_{HV} is caused by the fact that more than one virion are	(Marchuk et al., 1991)

15

			required to infect a healthy cell.	
γ_{HV}	0.34	Rate constant of epithelial cells infected by IAV	The difference between γ_{VH} and γ_{HV} is caused by the fact that more than one virion are required to infect a healthy cell.	(Marchuk et al., 1991)
b_{HF}	0.01	Rate constant of epithelial cells' virus resistant state induction		(Bocharov et al., 1994)
b_{IE}	0.066	Rate constant of infected epithelial cells that CTL damage	A single effector cell can deliver approximately 10 lethal hits.	(Bocharov et al., 1994)
a_I	1.5	Rate constant of infected epithelial cells damage by cytopathicity of IAV	The life time of an infected cell is approximately 1 day	(Zdanov et al., 1969)
b_{MD}	1	Rate constant of stimulation of antigen presenting cells by dead cells		(Marchuk et al., 1991)
b_{MV}	0.0037	Rate constant of stimulation of antigen presenting cells by virus particles		(Marchuk et al., 1991)
a_M	1	Rate constant of stimulated state loss of antigen presenting cells		(Marchuk et al., 1991)
b_F	250000	Interferon (IFN) production rate per APC		(Bocharov et al., 1994)
c_F	2000	Interferon (IFN) production rate per infected cell.	interferon α and β (IFN) are secreted also from infected cells(Julkunen et al., 2000)	Estimated
b_{FH}	17	Rate constant of epithelial cells that IFN binds		(Bocharov et al., 1994)
a_F	8	Rate constant of IFN's natural decay		(Bocharov et al., 1994)
b_{EM}	8.3	Rate constant of stimulation of effector cells		(Marchuk et al., 1991)
b_{EI}	2.72	Rate constant of death of effectors by lytic interactions with infected epithelial cells	A single effector cell can kill about 100 infected cells.	(Bocharov et al., 1994)
a_E	0.4	Rate constant of natural death of effector cells		(Marchuk et al.,

				1991)
b_{PM}	11.5	Rate constant of plasma cells production		(Marchuk et al., 1991)
a_P	0.4	Rate constant of natural death of plasma cells		(Marchuk et al., 1991)
b_A	0.043	Antibody production rate per plasma cells		(Marchuk et al., 1991)
γ_{AV}	146.2	Rate constant of antibodies which binds to IAV		(Bocharov et al., 1994)
a_A	0.043	Rate constant of natural death of antibodies		(Marchuk et al., 1991)
r	3e-5	Rate constant for S variable		Estimated

2.5   RESULTS

2.5.1   Standard Behavior

The standard behavior describes the course of infection in a naïve host. We assume that initially the host has no dead, infected or resistant cells, no interferon molecules, and no activated APC (i.e., H(0) = 1, I(0) = M(0) = F(0) = R(0) = 0). The initial levels of effectors, plasma cells, and antibodies are assumed to be at the homeostatic values (i.e., E(0) = P(0) = A(0) = 1) (Asquith et al., 2003). The influence of antigenic compatibility S on the progression of infection

17

is described in the subsection "Impact of Antigenic Distance" below. In a naïve host, we assume that $S(0) = 0.1$ which corresponds to a relatively low compatibility with the virus strain, that may have resulted from previous exposure to IAV and subsequent genetic drift. In the typical course of acute IAV Infection, the initial concentration of aerosol delivered virus particles that the host receives is about 10^6 particle per ml on day 0, corresponding to $V(0) = 0.01$ in our dimensionless system.

The resulting time courses of model variables corresponding to naïve infection are depicted in Figure 2-2. As seen in Figure 2-2, virus level peaks (period of maximum antigen concentration) after 5 days. This relatively late onset of the disease is the result of relatively low initial viral load used in our simulation. Peak viral load is increased by 10^4 fold with respect to initial value staying at peak approximately 3 more days, in accord with experimental data (Tamura et al., 1998). Viral load starts to decline to inoculation level after day 8 (early stage of recovery, disappearance of IAV particles). The host is considered infectious when the virus level exceeds 1, which happens at day 4.9. The host remains infectious for 2.6 days. APC are activated after 5 days peaking after about 7 days and returning to homeostatic levels within 8-10 days.

The resulting loss of respiratory epithelial cells (dead cells) is one major reason for several of the symptoms that accompany infection, such as cough, depressed tracheobronchial clearance, and altered pulmonary function (Hayden et al., 1998). We consider the host "symptomatic" if the damage level exceeds 10% of the epithelial cells(Marchuk et al., 1986), which occurs when the viral load peak at day 5. The maximum proportion of dead cells is 36% attained at day 6.1. The host stays symptomatic for 2.4 days after which time most of the cells become resistant to the infection. Infected cells reach a maximum proportion of 53% of all cells after day 5.2, while the proportion of resistant cells peak after 9 days, which is in accord with the

experimental observation that the expression of nucleoprotein (NP) mRNA in epithelial cells, showing the presence of infected cells, changes in parallel with viral titer (Fig. 2-2) (Tamura et al., 2004).

Interferon response comes into play once the virus peaks at day 5 making most of the cells resistant to infection. Interferon level is increased by 10^4 fold peaking approximately at day 6. Plasma cells are produced after 6 days peaking at 9 days, before virus-specific antibodies are detectable, in accord with empirical observations (Ada et al., 1986). Antibody production by plasma cells begins at day 7. There is a 10^3 fold increase in the amount of antibodies when the adaptive immune response comes into play to remove all viral particles and generate immune memory. Furthermore, antigenic compatibility is increasing monotonically starting right after when the adaptive immunity is activated (after day 8) and the antibodies are capable of inhibiting viral particles with 80% probability after 15 day of infection.
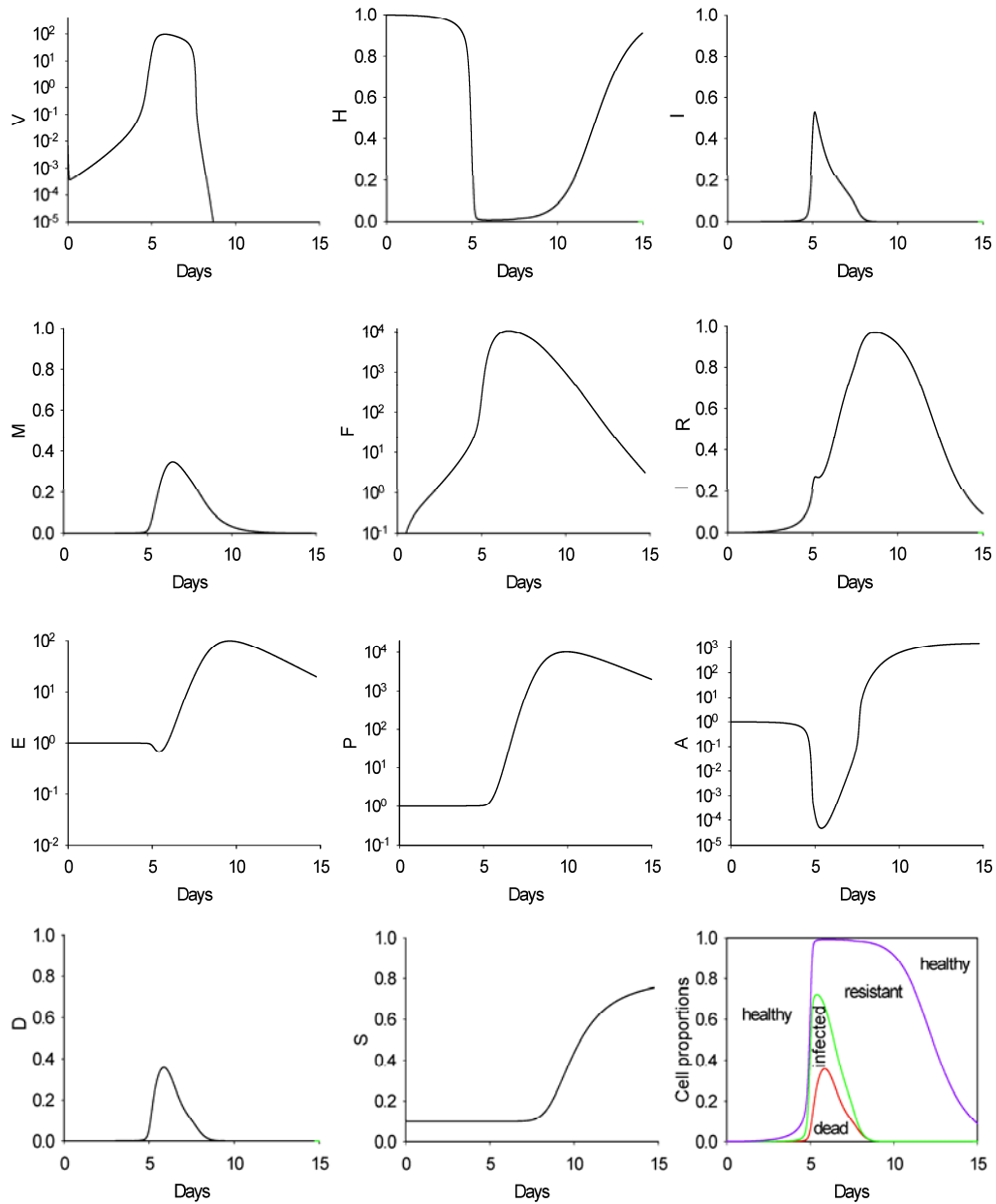
Figure 2-2. Time-courses of the viral load, proportion of respiratory epithelial cells, and the three arms of the immune response for a standard course of the disease.
Initially, the viral load is V(0) = 0.01, all cells are healthy, levels of APC and interferons are zero, effector cells, plasma cells and antibodies are at their homeostatic levels, and antigenic compatibility S(0) = 0.1. Panel at the bottom on the right displays cumulative proportions of types of respiratory epithelial cells: at any given time, below the red curve is the proportion of dead cells, between red and green the proportion of infected cells, between green and blue the proportion of resistant cells, and above blue is the proportion of healthy cells.

2.5.2 Impact of viral load

We investigated the impact of initial viral load on the onset, duration and severity of infection to understand the immune response of a naïve host to a moderate virus strain. It has been realized that IAV infection could result in large spectrum of disease states, however, this spectrum of severity has not been understood well (Yetter et al., 1980).

As seen in Fig. 2-3, the immune response falls into one of three categories depending on initial viral load, $V(0)$: asymptomatic disease, typical disease, and severe disease (Asquith et al., 2003). If $V(0)$ is less than the threshold V_1, the disease never develops. This corresponds to asymptomatic infection in which no virus shedding is observed. The host is considered not contagious in this case since the virus is eliminated from the host promptly and viral load remains very low with almost no ensuing damage. If $V(0)$ is in the range between V_1 and V_2, the disease follows the same trajectory but the larger $V(0)$ the sooner the onset of the disease. In other words, in this range of $V(0)$, the maximum viral load ($V_{max} = 138$), maximum damage ($D_{max} = 36\%$), the duration of symptoms, and length of contagious period are all *independent* of $V(0)$. If $V(0)$ is larger than V_2, the disease state corresponds to severe disease for which the maximum viral load and damage increase with $V(0)$. In this case maximum damage can exceed 50% of the respiratory cell population. Such levels of damage represent serious situation in which secondary infections could develop resulting in the death of the host. For standard parameter values the thresholds are $V_1 = 0.00227$ and $V_2 = 0.1$, with V_1 producing a trajectory terminating at a saddle node (see below), and V_2 being an approximate quantity determined as the lowest value of $V(0)$ for which the trajectory perceptibly departs from the typical behavior.
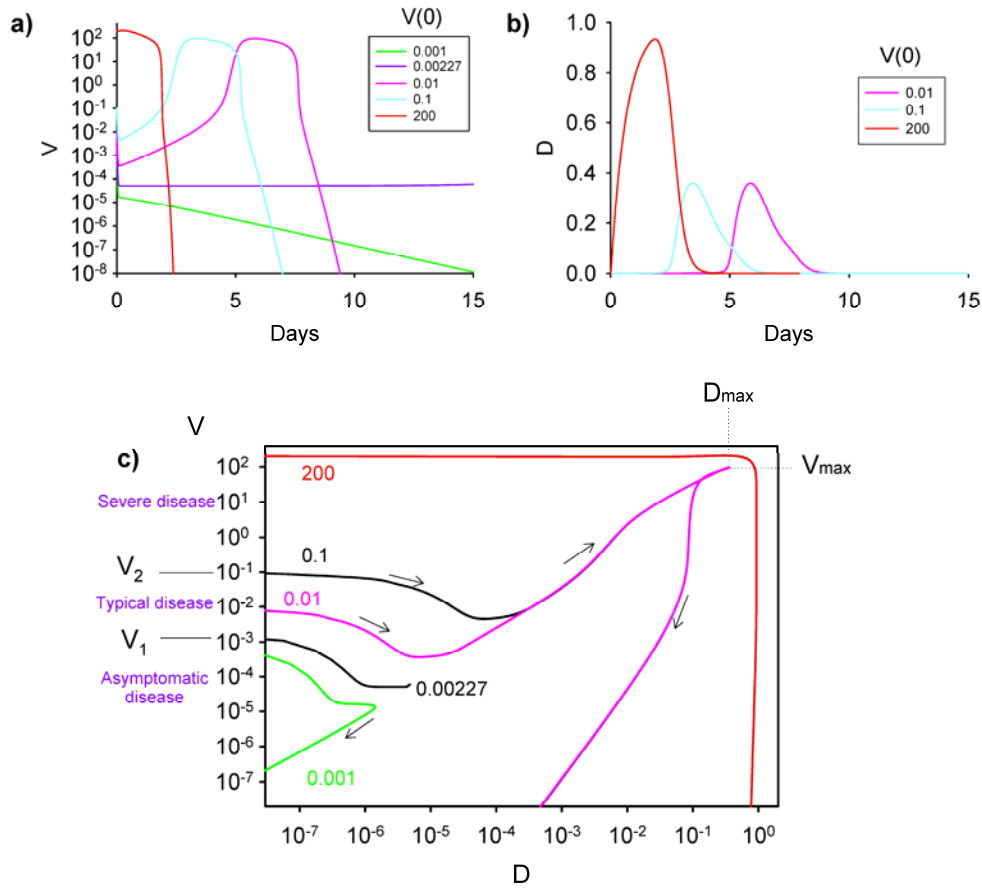
Figure 2-3. Time-courses of (a) viral load and (b) damage for various levels of the initial viral load V(0).
For V(0) in the range from 0.00227 to 0.1 the dependence of V on t (and of D on t) follows the same trajectory but the larger V(0) the sooner the onset of the disease. (c) phase diagram of the dependence on initial viral load V(0) as a plot of log V versus log D. The direction of time is indicated by arrows. The maximum viral load and maximum damage for typical disease are $V_{max} = 1.3 \times 10^{10}$ particles/ml and $D_{max} = 36$. The thresholds $V_1 = 0.00227$ for the typical disease and $V_2 = 0.1$ for the extreme disease are indicated and the corresponding trajectories are shown in black.

22

Fig. 2-3(c) shows the projection of the phase diagram onto the variables V and D. In this projection the trajectories have only a very limited tendency to cross. The trajectories for initial conditions $V_1 < V(0) < V_2$ all coincide, in accord with the observation that the trajectories are very similar and only shifted in time. On this plot the trajectory with $V(0) = V_1$ terminates at the point $(V,D) = (0.0015, 0.0001)$. Note that because the graphs are plotted on a logarithmic scale and $D(0) = 0$, the trajectories originate off the graph on the left.

2.5.3   Stability analysis

As expected, the flow of the dynamical system defined by (1)-(11) leaves invariant the physiological region of the phase space obeying $0 \leq (V, F, E, P, A)$, $0 \leq (H, I, R, D, S, M) \leq 1$. Within that region, for the baseline parameter values, the system (1)-(11) with parameters as in Table 2-2 has 3 steady states. One is the healthy steady state x_h at which (V, H, I, M, F, R, E, P, A,S) = (0, 1, 0, 0, 0, 0, 1, 1, 1, 1), the second is a threshold state x_{th} for which (V, H, I, M, F, R, E, P, A, S) = (0.0014698, 0. 9865, 0.00031472, 0.00012869, 1.3243, 0.013064, 1.0005, 1.0037, 0.16739, 1), and the third one is a high-virulence state x_v for which (V, H, I, M, F, R, E, P, A, S) = (2.9646, 0.0903, 0.056947, 0.034516, 916.91, 0.82797, 1.49024, 130.29, 0.012925, 1). The threshold state corresponds to the separator for the dynamics of influenza between the asymptomatic disease and typical disease cases as seen in Fig. 2-3. The Jacobian matrix for the linearization of the system (1)-(11) about the healthy state x_h admits eigenvalues that are all real and negative, and hence the healthy fixed point is asymptotically stable. We find that, with the exception of a small number of cases, the healthy state remains stable under perturbations of the

23

parameters of the system. The Jacobian matrix for the threshold state x_{th} has two complex and one positive eigenvalue and hence x_{th} is a saddle node. The Jacobian matrix for the high-virulence state x_v has one positive eigenvalue and hence x_v is also a saddle node. As discussed below, the x_v becomes stable at fixed, extremely low values of S(0).

2.5.4   Sensitivity analysis

The goals of sensitivity analysis with respect to random perturbations of the model parameters are the following:

- To show how robust the simplified uncomplicated influenza model is in relation to perturbed parameter values.

- To explore to which parameters the system is more sensitive to understand key processes and immune system mechanisms.

Our approach to investigate sensitivity was based on studying the effect of changes in the parameters (in every case we increased and decreased the baseline value threefold) on the duration, onset and severity of the disease. In clinical studies, the assessment of influenza virus pathogenicity is based on the magnitude and duration of fever, the frequency and amount of virus shedding, and the level and persistence of the infection. Within the model framework we can generalize these clinically relevant correlates into the following characteristics: (I) the *severity* of the disease measured as the maximum attained proportion of dead cells. $D_{\max} = \max_{t>0} D(t)$, (II) the *duration* of symptomatic infection $\Delta t_{illness}$=t$_2$-t$_1$, where t$_1$ is the time that D exceeds 0.1 and t$_2$ is the time that D drops below 0.1 (III) similarly, the value V =1 is considered to be the threshold

24

level for becoming contagious and the duration of *infectivity* will be referred to as $\Delta t_{\text{contagious}}$. For

typical disease, we find that $\Delta t_{\text{illness}}=2.4$ days and $\Delta t_{\text{contagious}}=2.6$ days.

Table 2-3. One-way sensitivity analysis on model parameters.

Parameter	Baseline (range)	Model behavior
γ_{HV}	.34 (.1-1)	• At high virulence, disease always develops. At low virulence, asymptomatic disease is possible. • The higher the virulence, the earlier the onset of disease. • The higher the virulence, the shorter the duration of disease. • At high virulence, damage ($D_{max}=68\%$) is at least five times larger than that of low virulence ($D_{max}=12\%$). So, high virulence may cause death. • At peak, virus shedding is about the same for high and low virulent viruses. • The less virulent the virus, the longer the contagious period when disease is developed.
γ_V	510(150-1500)	The model behavior is same as in case for γ_{HV}.
γ_{VA}	619.2(200-1800)	• For low γ_{VA}, disease always develops. • The higher the γ_{VA}, the later the onset of disease. • At high and low values of γ_{VA}, the duration of disease is about the same. • At high and low values of γ_{VA}, the damage is about the same. At peak, virus shedding is about the same for high and low γ_{VA}. • The contagious period is about the same for various values of γ_{VA}. So, γ_{VA} only affects the onset of the disease which has same characteristics.
b_{MD}	2(0.6-6)	• Disease always develops for all b_{MD}. • The onset of disease stays the same. • The higher b_{MD}, the shorter the duration of disease. • The higher b_{MD}, the lesser the damage. Very low values of b_{MD} may cause death. At peak, virus shedding is about the same for high and low b_{MD} • The higher b_{MD} the shorter the contagious period. • If b_{MD} is very high the onset is very late, duration is short, damage is very low, contagious period is very short.
b_{IE}	0.066(0.02-0.1)	• At high b_{IE}, asymptomatic disease is observed for standard V(0) and S(0). • The higher b_{IE}, the later the onset of disease. • The higher b_{IE}, the shorter the duration of disease. • At high values of b_{IE}, the damage is lower. Changes only in b_{IE} only can not cause death.

		• At peak, virus shedding is about the same for high and low b_{IE}. • The higher b_{IE}, the shorter the contagious period when disease is developed.
a_I	1.5(0.5-4.5)	• At high a_I, asymptomatic disease is observed for standard V(0) and S(0). • The higher a_I, the later the onset of disease. • The higher a_I, the shorter the duration of disease. • At high values of a_I, the damage is lower. Changes only in b_{IE} only can not cause death. • Virus shedding is very sensitive to a_I. When a_I is higher, at the peak viruses shed less. • The higher a_I, the shorter the contagious period. But the time difference is very small.
b_{HD}	4(2-8)	• Disease always develops for all b_{HD} for standard V(0) and S(0). • Onset of disease is about the same for all b_{HD}. • The higher b_{HD} the shorter the duration of disease. • At high values of b_{HD}, the damage is lower. Changes only in b_{HD} can not cause death. • Virus shedding is very sensitive to b_{HD} When b_{HD} is higher, at the peak viruses shed more. • The higher b_{HD}, the longer the contagious period. The time difference is significant.
b_F	25000(125000-500000)	• Disease always develops for all b_F for standard V(0) and S(0). • Onset of disease is the about same for all b_F. • The higher b_F, the shorter the duration of disease. • At high values of b_F, the damage is lower. Very low values of ρ_G may cause death. • Virus shedding is very sensitive to b_F. When b_F is higher, at the peak viruses shed less. • The higher b_F, the longer the contagious period. The time difference is significant.
b_A	0.043(0.01-0.12)	• Disease always develops for all b_A for standard V(0) and S(0). • The higher the b_A, the later the onset of disease. • The duration of disease is about the same for all b_A. • At high values of b_A, the damage is lower. Changes only in b_A can not cause death. • Virus shedding is sensitive to b_A. When b_A is higher, viruses shed a little at the peak less. • The higher b_A, the shorter the contagious period. The time difference is small.

b_{HF}	0.02(0.005-0.03)	• At high b_{HF}, asymptomatic disease is observed for standard V(0) and S(0). • Onset of disease is about the same for all b_{HF}. • The higher b_{HF}, the shorter the duration of disease. • At high values of b_{HF}, the damage is lower. Very low values of b_{HF} may cause death. • Virus shedding is very sensitive to b_{HF}. When b_{HF} is higher, at the peak viruses shed significantly less. • The higher b_{HF}, the longer the contagious period. The time difference is significant.
b_{EM}	8.3(2.5-25)	• At high b_{EM}, asymptomatic disease is observed for standard V(0) and S(0). Onset of disease is about the same for all b_{EM}. • The higher the value of b_{EM}, the shorter the duration of disease. • At low values of b_{EM}, the damage is lower. Very high values of may cause death. • Virus shedding is not sensitive to b_{EM}. • The higher the value of b_{EM}, the shorter the contagious period. The time difference is not significant.
b_{PM}	11.3(3-30)	• For low values of b_{PM}, flow goes through disease trajectory and converges to the fixed point for standard V(0) and S(0). • Onset of disease is about the same for all b_{PM}. • The duration of disease is about the same for all b_{PM}. • The damage is about the same for all b_{PM}. • Virus shedding is not sensitive to b_{PM}. • The higher the value of b_{PM}, the shorter the contagious period. The time difference is significant.
S(0)	0-1	• For S(0)=0 disease always develop for standard V(0). • The higher the S(0), the later the onset of disease. The duration of disease is about the same for all S(0). • At high values of S(0), the damage is lower. When S(0) is higher, viruses shed less at the peak. The higher the value of S(0), the higher the contagious period during the typical disease.

2.5.4.1 Sensitivity to pathogen virulence

Virulence is characterized by the parameters γ_{HV} and γ_V, which represent the rate of infection of epithelial cells by IAV and the rate of IAV particles secretion per infected epithelial cell, respectively. When virulence is high, the viruses are able to infect the healthy cells at much higher rate and they reproduce and replicate themselves in infected cells much faster. Since the sensitivity to γ_{HV} and γ_V are essentially the same, we will consider only parameter γ_{HV}.

The virulence γ_{HV} affects the range of viral loads $V(0)$ causing typical disease. When the value of γ_{HV} is three times more than the baseline value, then no matter what the initial viral load is, disease always develops (See Fig. 2-4(b)). When γ_{HV} is three times less then the baseline, we observe the presence of asymptomatic, typical and severe disease regimes depending on $V(0)$. When $V(0)$ is low, the disease stays asymptomatic. The higher the virulence, the earlier the onset of disease and the shorter the duration of disease. The variation in maximum damage, m_{max}, between the case of low γ_{HV} and the case of high γ_{HV} is significant (we found a fivefold difference between $D_{max} = 68\%$ for $\gamma_{HV} = 1$ and $D_{max} = 12\%$ for $\gamma_{HV} = 0.1$). As expected, infection by virus of high virulence causes substantial damage, while infection by a virus of low virulence may go unnoticed. The lower the virulence, the longer the contagious period $\Delta t_{contagious}$. The duration of the disease and maximum level of virus titer at the peak are not sensitive to the virulence. When γ_{HV} is 0.1, the threshold value for $V(0)$ to cause typical disease is 0.00227. The
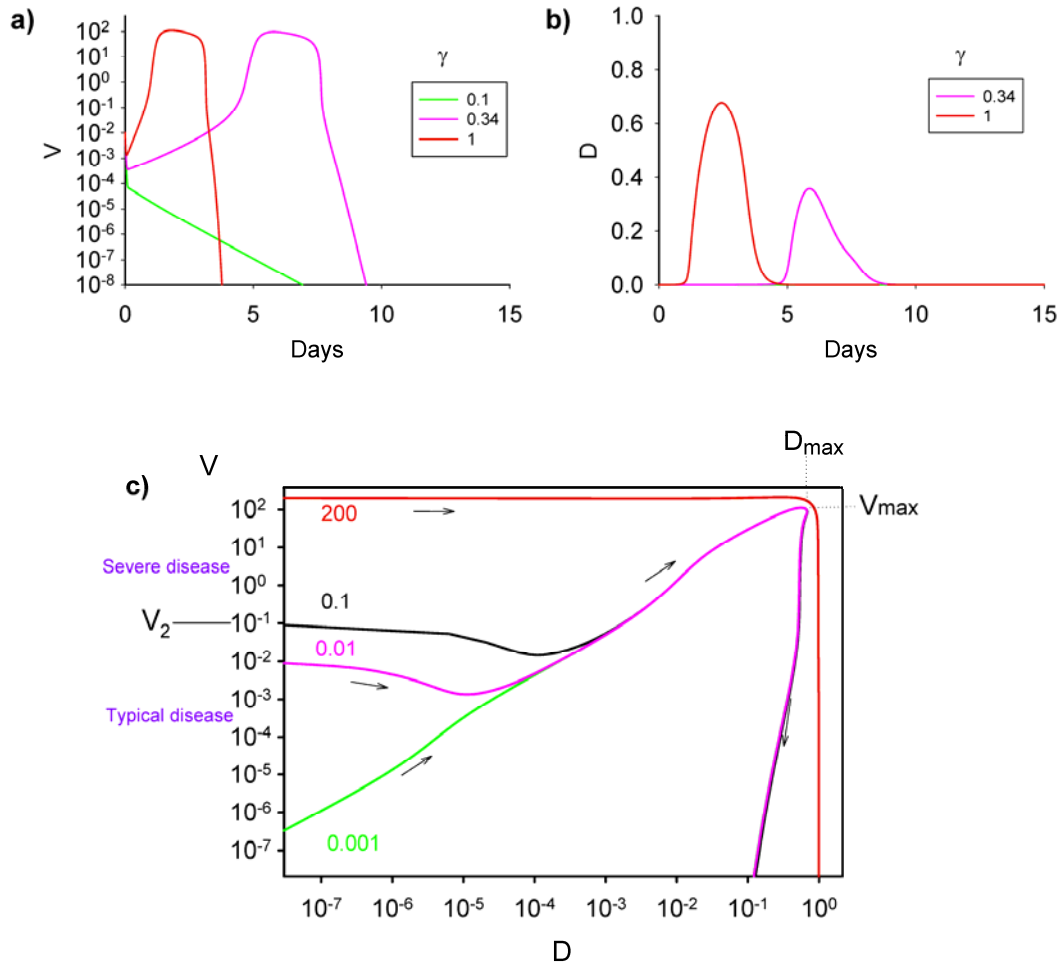
Figure 2-4. Time-courses of (a) viral load and (b) damage for various values of γ_{HV}. (c) phase diagram of the dependence on initial viral load V(0) for value of γ_{HV} (γ_{HV} =1) that is 3 fold higher than the standard value.
The direction of time for each curve is indicated by arrows. The maximum viral load and maximum damage for typical disease are $V_{max} = 1.1 \times 10^{10}$ particles/ml and $D_{max} = 68$.

phase diagram for γ_{HV} is 0.1 (not shown) is essentially the same as Fig. 2-3(c). The threshold point of the dynamics between the typical disease case and the asymptomatic case is due to the presence of an unstable threshold state x_{th} which stable manifold intersects the locus of initial conditions.

2.5.4.2 Sensitivity to interferon response

The parameters b_F and b_{HF} characterize the interferon production rate constant and the rate constant of induction of resistant state in epithelial cells, respectively. If b_F increased or lowered from its standard value, disease always develops for standard values of $V(0)$ and $S(0)$. However, when b_{HF} is high, the host remains asymptomatic. The time of onset of disease does not depend on b_F and b_{HF}, but when either of these constants are higher, the duration of disease becomes shorter. Damage increases if either b_F or b_{HF} is decreased. Very low values of b_F or b_{HF} result in excessive damage (over 50%) which may presumably lead to secondary infections or death (Iwasaki et al., 1977). Virus shedding is sensitive to the magnitude of b_F or b_{HF}: higher values are associated with a less virus shedding but a longer contagious period. When the interferon production rate constant is two times bigger than the baseline value (i.e., when b_F=500000), then the host remains contagious for about 3.5 days. When this rate is two times less than the baseline (i.e., when b_F=125,000) then the contagious period is about 2.3 days. So, the difference in the length of infectious period is significant for various levels of innate immune response.

Even in the absence of an innate response (when b_F=0 and b_{HF}=0), the disease is eventually healed by the adaptive immune response and the organism will approach the healthy state.

2.5.4.3 Sensitivity to cellular component of innate immunity

The parameters b_{EM} and b_{IE} stand for the rate constant of production of effector cells and rate constant of removal of infected cells by effectors, respectively. For sufficiently large b_{EM} or b_{IE}, the host is able to clear the disease without symptoms and typical disease conditions, given the standard initial immunity and standard initial amount of the virus. Although b_{EM} has no effect on the onset of the disease, when infected cell removal rate constant is high, the onset of infection happens later. At low values of b_{EM} or b_{IE}, the symptoms last longer. When b_{EM} is high, the resulting maximum damage, D_{max}, is large and may result in death. On the other hand, when b_{IE} is high, we observe lower damage of epithelial cells. Even under a significant decrease in b_{IE}, D_{max} will stay under 50% and hence a decrease in in b_{IE} has no effect on the mortality. Virus shedding is the same for different levels of b_{EM} or b_{IE}. When there is a less vigorous cellular response, the host remains infectious for longer. But the time differences in the contagious period of the host for various levels of b_{EM} or b_{IE} are small.

Even in the absence of a cellular response (when $b_{EM}=0$ and $b_{IE}=0$), virus is eventually cleared by the innate and adaptive immune responses and the organism will approach the healthy state.

2.5.4.4 Sensitivity to adaptive response

Activation of adaptive immune response is slower than activation of cellular and interferon components of innate immunity. The parameters b_{PM}, b_A and γ_{VA} stand for the plasma cell production rate constant, antibody production rate constant and the rate constant of neutralization of IAV by antibodies. For sufficiently large b_{PM}, b_A or γ_{VA}, the host is able to clear infection without symptoms after administration of a standard inoculum. Although b_{PM} has no

effect on the onset of the disease, later onset is observed with higher b_A and γ_{VA}. The duration of illness does not depend on b_{PM}, b_A or γ_{VA}. Damage is lower with higher b_A, while damage is insensitive to the two other rate constants. Variations in b_{PM}, b_A or γ_{VA} never result in excessive damage. Virus shedding is sensitive to b_A. With higher b_A, less virus is shed at the peak of the disease and the contagious period is significantly shorter.

In summary, γ_{VA} only affects the onset of the disease, while b_{PM} affects only virus shedding at the peak. The system is much more sensitive to the b_A. We'll discuss the situation where there is no adaptive response or very weak response in the next subsection.

2.5.4.5 Impact of Antigenic Distance

The efficiency of the existing antibodies of the organism to neutralize the virus of the strain causing the illness is represented by the variable S which describes the probability of a match between the existing antibodies and the antigenic structure of the viral strain. Fig. 2-5(a) displays the dependence of incurred damage on $S(0)$, the initial value of S. Previous infection with one subtype induces little or no immunity to other subtypes of the IAV (Couch et al., 1983; Murphy et al., 1989), therefore $S(0)$ for the individual facing a new subtype is very low. For the standard value of $S(0)$, corresponding to the standard response, we chose $S(0) = 0.1$ which corresponds to partial match of antibodies due to the history of previous contacts of the individual with the virus, perhaps during the last season. This standard $S(0)$ is much lower than 1 because of the antigenic drift of the virus strain. When there is no initial match at all ($S(0)=0$), damage is higher (Yetter et al., 1980). When $S(0)$ is sufficiently large, then the individual

remains asymptomatic (Liew et al., 1984; Yoshikawa et al., 2004). As seen in Fig. 2-5(b), when

$S(0)=0$, disease always develops regardless of initial viral load, i.e., $V_1 = -\infty$. The threshold for
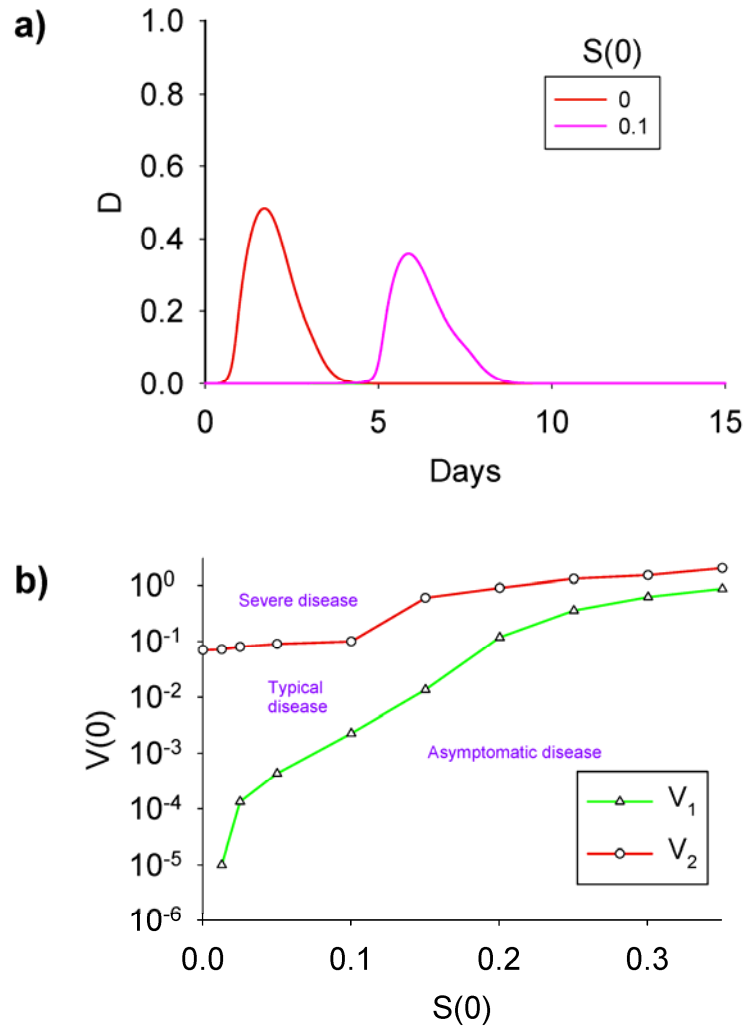
Figure 2-5. (a) Time courses of the damage for various levels of the initial probability of the existing antibodies to neutralize IAV particles, S(0). The larger S(0) the sooner the onset of the disease. (b) Diagram of the dependence of the expected type of disease on V(0) and S(0).
The lines correspond to the threshold values V_1 (triangles connected by green lines) and V_2 (circles connected by red lines). The regions corresponding to asymptomatic, typical and severe disease are indicated.
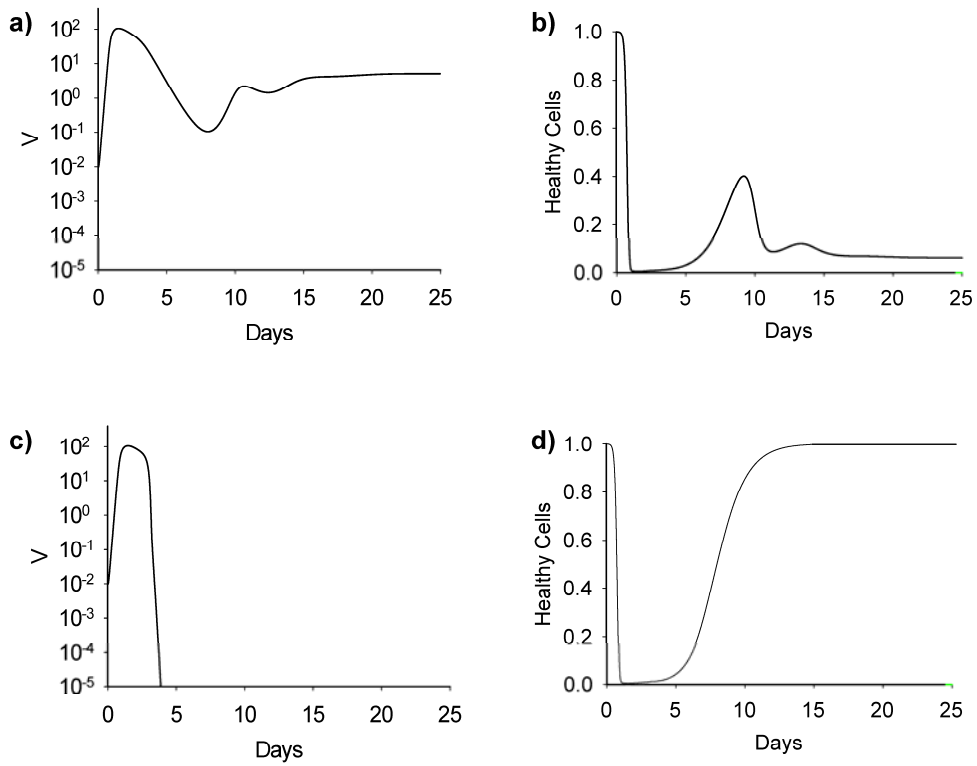
Figure 2-6. Time-courses of (a) the viral load and (b) the proportion of healthy cells for an individual with no initial and no improvement in antibody compatibility, $S(0) = 0$, $r = 0$, i.e., an individual without adaptive immune response. Failure to develop compatible antibodies results in recurrence of the disease and transition to a chronic state. Time-courses of (c) the viral load and (d) the proportion of healthy cells in an individual whose existing antibodies are incompatible but improving, i.e., $S(0) = 0$, $r = 10^{-5}$. As virus-specific antibodies appear with the adaptive response, IAV particles are removed from the host completely.

severe disease, V_2, increases with S(0). The threshold for typical disease, V_1, becomes finite when S(0) = 0.0124 and then increases with S(0). For values of S(0) above 0.2, corresponding to reasonably compatible initial immunity, the disease is asymptomatic unless V(0) > 0.1. This situation corresponds to an immunized individual. The higher the S(0), the later the onset of disease. The duration of disease is about the same for all S(0). At high values of S(0), the damage is lower (Yetter et al., 1980) When S(0) is higher, shed viruses less at the peak. The higher the value of S(0), the less the contagious period (Yetter et al., 1980).

The parameter *r* controls the rate of improvement of antigenic distance. A zero rate r corresponds to the situation in which antibodies do not improve their ability to match antigens. Complete failure to develop antibodies (When S(0)=0 and r=0) results in recurrence of the disease and transition to a chronic state, as seen Fig. 2-6(a)-(b). This state is characterized by the following values: (V, H, I, M, F, R, E, P, A) = (5.26, 0.06, 0.018, 0.05, 1484, 0.89, 67.0). As the immune system produces virus-specific antibodies, the host is able to clear the disease even in the case when the production rate of compatible antibodies is quite low such as $r=10^{-5}$, as seen in Fig. 2-6(c)-(d). A partial failure to develop antibodies occurs when S(0) > 0 and r = 0. In that case, if S(0) is sufficiently small (below 10^{-7}), complete failure occurs, with recurrence of the disease and transition to a chronic state (not shown).

To obtain further insight into the influence of the variable S on the behavior of the system we considered the reduced system of equations (1)-(9) with S treated as a constant, and studied changes in the location and stability of fixed points of this reduced system as a function of S. The corresponding bifurcation diagram, shown in Figures 2-7(a)-(b), reveals that when S < S* = 0.000224555, the high virulence state x_v is stable while the healthy state is unstable. (This is compatible with the behavior of the full system for S = 0 and r = 0 described above). At S = S*,

37

a)

b)
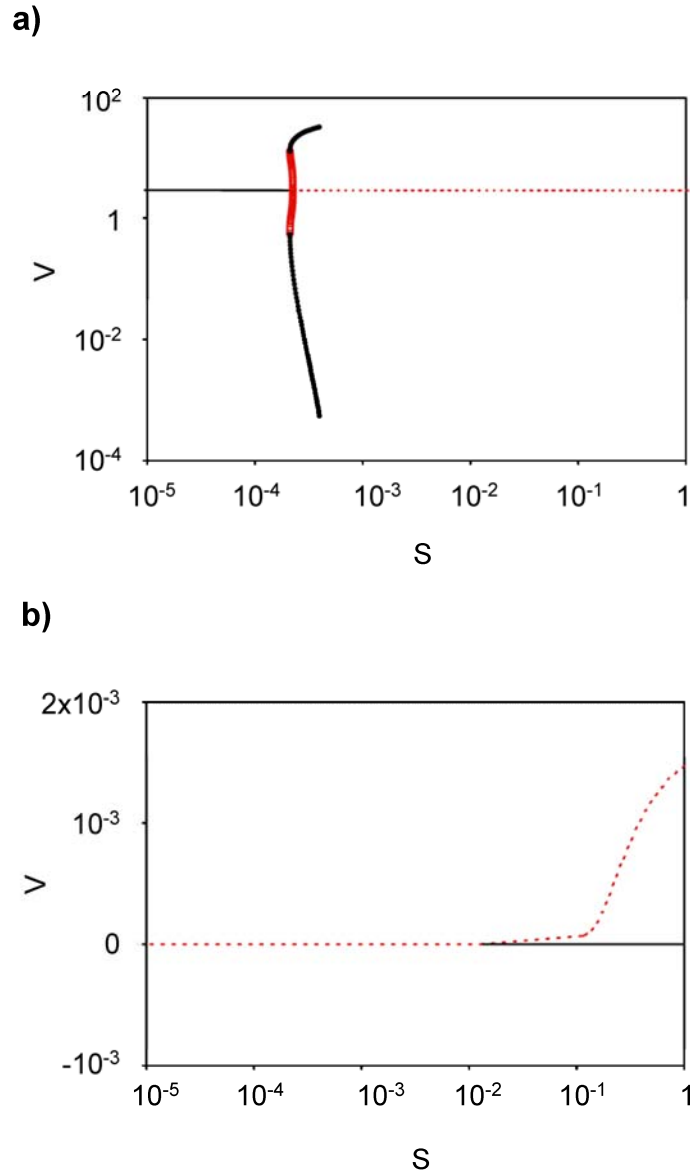
Figure 2-7. Bifurcation diagram for a reduced system of equations (1)-(9) with S treated as a bifurcation parameter.
Two separate parts of the diagram are shown: (a) the high virulence steady state and connected branches and (b) the healthy state and connected branches. Stable states are shown as solid black curves, unstable steady states as dashed red curves, unstable periodic orbit as hollow red circles and stable periodic orbit as solid black circles. (The branch of limit cycles is terminated due to difficulties in its numerical calculation, but is expected to persist up to the value $S = 1$.)

a subcritical Hopf bifurcation occurs which gives rise to a family of unstable periodic orbits. That family continues as a family of stable limit cycles for values $S > S^*$. (Only a portion of that branch is shown in Figure 2-7 (a); difficulties with numerical calculation of that branch prevent us from determining whether the stable limit cycle persists for all $S <= 1$.) The healthy steady state x_H is unstable until S reaches $S^\# = 0.0129294$, at which value x_H gains stability through a transcritical bifurcation. A branch of unstable threshold steady states x_{TH} bifurcates off of x_H and exists for $S > S^\#$.

2.6   DISCUSSION

We presented a simplified model of the human immune response to the IAV infection in individual hosts which includes innate and adaptive immunity, and analyzed its behavior. Such a model could be used to explore in more detail individual determinants of symptoms and behavior of clinical relevance, especially in large-scale simulations of disease spread and containment. Simulation and sensitivity analysis of this model suggest that for majority of possible parameter values and initial conditions the course of the disease falls into one of three categories: asymptomatic disease, typical disease, and severe disease. In special circumstances a recurrence of infection may occur, followed by a transition to either healthy or chronic state.   The magnitude of initial viral load V(0) determines which of the paths will be taken, in accord with experimental observations (Tamura et al., 2004). With sufficiently small viral inoculum, disease is asymptomatic in the sense that the virus level decreases monotonically to 0 and damage remains very low. With inocula within the interval of values corresponding to typical disease, virus shedding, duration of sickness and the severity of symptoms, as well as the duration of

contagious period are independent of size of inoculum; only the time of the onset of disease changes: disease peaks earlier for larger inocula. An important epidemiological implication of this result is that from observations of a typical disease it is impossible to determine a posteriori both when the infection occurred and what was the initial virus load since these data are interdependent. When the inoculum is sufficiently large (more than 0.1 particles per epithelial cell in some cases), disease becomes severe with maximum viral load and maximum damage increasing proportionally to the size of the inoculum.

Analysis of the adaptive immune response revealed that whenever there is sufficient antibody response with enough specificity, the dynamics will restore health, irrespective of the intensity of the innate responses and of the trajectory followed by the disease. However, if memory cells cannot produce sufficiently compatible antibodies against the IAV particles initially (very low $S(0)$) or cannot improve the antigenic compatibility sufficiently rapidly (S is not increasing during the disease), there is rebound of virus shedding and transition of the system to a chronic state.

The role of antigenic compatibility in virus clearance can be viewed as a series of transitions in the bifurcation diagram of Fig. 2-7, once one realizes that S is slowly, but steadily, increasing during the course of the disease in initially naïve individuals. Near $S = 0$ the healthy steady state is unstable and the system initially approaches the chronic state. Eventually, S increases beyond S^*, the limit of stability of the chronic state, and the system will approach the limit cycle. Eventually, S will increase beyond $S^\#$, at which instant the healthy state becomes stable and the immune system clears the infection.

The reduced model underlines the importance of antigenic distance between the virus strain which causes IAV infection and the existing virus-specific antibodies of the adaptive

response represented in the model by S variable. Children who previously experienced natural infection or who received a live virus vaccine exhibit a marked reduction in both the amount and duration of virus shedding when compared to subjects without prior exposure to IAV infection (Tamura et al., 2004). Compared with adults, children can shed virus earlier before illness begins and for longer periods once illness starts. In children absolute levels of virus shedding may be higher than those in adults. These experimental findings confirm our model predictions (see Fig. 5) which take into account the immune memory of the individual providing not only much accurate predictions for the host but also a solid foundation as individual-based model for realistic epidemic models. Our results suggest that in the absence of initial immune memory (low $S(0)$ or $S(0)=0$) due to lack of proper vaccination or new subtype of the virus, the individual would experience severe disease which might result in death and remains contagious for a longer period of time. Therefore, such an individual has a larger probability to die and spread the disease in an epidemic.

Our results illustrate the point that IAV infection caused by highly virulent viruses may cause death due to substantial damage, while infection by a virus with low virulence may be cleared without any symptoms: a combination of viral properties and host susceptibility determines the outcome of infection(Price et al., 2000). High virulence corresponds in our model to high values of the parameters γ_{HV} and γ_V which characterizes the rate of infection of epithelial cells by IAV and the rate of IAV particles secretion per infected epithelial cell, respectively. In the three global pandemic of the last century, new subtypes with higher values of γ_{HV} and γ_V arose due to antigenic shift. Since there was no or very little immunity of human population to these new subtypes (0 or very low $S(0)$) combining with high virulence, they caused excessive mortality rates with large probability of death for particular individuals as our results indicated.

41

Although the H5N1 subtype of avian flu has very limited ability to bridge the species barrier and humans to human has not been observed(Kuiken et al., 2006; Shinya et al., 2006), it might mutate into a form for which it can be transmitted from human to human. Since this new subtype (i.e very low $S(0)$ for individuals) of the IAV is very virulent (i.e. γ_{HV} and γ_V both high), it would be predicted to cause excessive damage in individuals, conditions conducive to a pandemic. Containment measures should be taken such as antiviral drugs which can neutralize the actions of NA (i.e. decreased γ_V) and efficient vaccination which can improve host immunity by the existence of very affine subtype specific antibodies neutralizing the actions of HA (i.e very low $S(0)$ and decreased γ_{HV}). Sensitivity analysis of the model suggest that innate response is an early, important line of nonspecific defense which has significant impact on lowering the duration of sickness, virus shedding and tissue damage. Contagious period of an individual which is an important measure for disease control is increased by the higher interferon response. Sensitivity analysis also suggests that higher cellular response result in lower period of symptomatic case and contagious period.

Although each component of innate and adaptive immune response contributes to the recovery of IAV infection, the simulations suggest that, in the absence of one component of innate immunity, the remaining two defense mechanisms are sufficient for viral clearance. For example, when cellular component are not involved in viral clearance, antibodies (sufficient in the amount and affinity) on their own can mediate clearance of influenza (Scherle et al., 1992). The cellular response can also be sufficient to clear the IAV infection from an individual (Asquith et al., 2003). In the absence of adaptive immunity, the viral load is brought down to very low levels, although not completely cleared, which is supported by experiments showing that in some circumstances antibody response is necessary to clear the infection (Iwasaki et al.,

42

1977). For example, in nude mice without antibodies the viral particles survive with chronic infection (see Fig. 2-6(a)) (Scherle et al., 1992). After transferring T helper cells into the infected mice that promotes antibody response, the disease is completely cleared (Iwasaki et al., 1977; Scherle et al., 1992). Therefore, one can conclude that innate defense mechanisms are not capable of curing the disease on their own in the absence of antibody response, and can only reduce the disease to a chronic state (see Fig. 2-6(b)). Host may escape from this chronic state with sufficient adaptive response or through sufficient cellular response (Epstein et al., 1998).

The biological relevance of our analysis and conclusions are limited by the significant oversimplification present in our reduced model and the difficulty in translating functions such as "antigen presenting cells", "damage", "effector cells" into measurable quantities as we have done in more specific models.(Chow et al., 2005) Our model does not permit the derivation of the number of new cases per infected cases, or R_0. Yet, inscribed in a simulation furnishing distributions of viral loads/contact and contact density, such a number could be derived. Future development of the biological model include detailed mathematical analysis of the system of equations of the model, correlating infectivity and classes of symptoms to specific components of the model such as viral load, interferon levels and proportion of unhealthy respiratory epithelial cells, and improved biological fidelity and calibration data. We wish to include the effects of age and genetic variations through realistic distributions of key model parameters. Such an extension will be used to conduct large scale simulations of clinical trials of antiviral strategies in genetically heterogeneous hosts and to construct response surfaces to be integrated in multiscale models of IAV infection.(Clermont et al., 2004) We also wish to develop a more sophisticated model of antigenic distance.

3.0   ENSEMBLE MODELS FOR HUMAN IMMUNE RESPONSE TO INFLUENZA VIRUS INFECTION

3.1   INTRODUCTION

Mathematical models are essential tools in disease modeling that help in making predictions about the outcome given the characteristics of the pathogen and immune state of the host. Majority of models in mathematical biology are traditionally deterministic in nature. These deterministic models sufficiently capture the average behavior of the biological system under consideration. However, they are not capable of describing the stochastic characteristics of the underlying system. The rate constants (parameters) in these deterministic models representing the chemical reactions between model variables are usually picked (sometimes by guess) in a big range of possible values to fit the model to the biological observations. In the deterministic model in (Hancioglu et al., 2007) and Chapter 2, we generated a set of parameter values as given in Table 2-2, which describes the process of immune response to influenza virus infection. This set is chosen to fit the model to the observations given in(Bocharov et al., 1994; Hayden et al., 1998). The values chosen are neither the best nor the most "effective" ones corresponding to the chemical reactions happening in the upper respiratory tract mucosa.

In order to understand the stochastic nature of the events happening in the components of the immune system and the probabilistic outcome, we need a different modeling approach taking into account the random characteristics of the pathogen (a priori the specific virus strain for future influenza outbreak is not known) as well as the host (vaccinated versus unvaccinated or immunosuppressed, etc.). Since the deterministic model is not able to capture the probabilistic nature of individual immune responses to influenza viruses (no statistical analysis may be done based on it), a model providing probabilistic predictions to quantify individual variability of the immune response to specific virus characteristics is a crucial need. The purpose of the stochastic model is not limited to account for random phenomena regarding variable individual responses to different strains. It also provides population level statistics of symptom development, infectiousness, mortality rates, duration of disease and most importantly it suggests the best treatment and containment strategies for the susceptible population.

Modeler may choose different paths to reach these objectives and to incorporate stochasticity into the deterministic approach. We chose modeling human immune response to influenza infection by an ensemble model to incorporate the stochastic effects mentioned above. In this part, instead of having one set of parameters for model equations, we construct model ensembles that vary in parameter values and ranked according to their likelihood to capture existing data or clinically available observations. An ensemble prediction contains multiple runs of numerical prediction models, which differ in the initial conditions, model structure or parameter values addressing the major sources of uncertainty(Gneiting et al., 2005). We focus on the uncertainty coming from the parameter values in our ensemble model approach. So, we extend the deterministic ODE model obtained in the previous chapter to an ensemble model so as the information inferred from an a priori knowledge is used to obtain an a posteriori distribution

which contains all the information on the model space. Our main goal is to quantify uncertainty in model predictions due to parameter heterogeneity.

In most of the epidemiological models, the immune response to pathogen interactions has been considered as an intrinsically deterministic endeavor. Ensemble models have been widely used in large scale simulations of weather systems as well as dynamical models of microbial cell population to account for the uncertainty connected with the design of models, estimation of model parameters and the heterogeneity of parameters across a population. Probabilistic forecasts in these weather models allow one to quantify weather related risk, and they have greater economic value than deterministic forecasts in a wide range of applications including disease modeling (Gneiting et al., 2005). Similar approach that is used in weather predictions may be applied to model biological systems, processes, disease spread and in particular immune response to pathogen. The results obtained through simulations of an ensemble model are the probabilistic predictions of the dynamics that accurately represents the variability of responses in individuals.

We have adopted a similar approach with the exception that the source of our uncertainty lies mainly in parameter estimation on sparse datasets, yielding an ensemble of models differing *not* by their initial conditions or equation structure (typically the case in weather models), but by model parameters. We achieved a characterization of the joint probability densities of these parameter sets, based on empirical data and observations. We believe that from individual level to multiscale population level models, ensemble methods may potentially become a prominent part of numerical disease modeling. Indeed, probabilistic predictions based on reasonably well characterized probability densities of parameter sets would provide the best account for the uncertainty observed in individual immune responses against influenza viruses.

46

3.2   MATHEMATICAL MODEL DEVELOPMENT

3.2.1 Posterior distribution

Parameters in empirical mathematical models are determined from available experimental data using a process called regression. Parameters of the ODE model, the underlying deterministic model representing the human immune response to IAV infection, in (Hancioglu et al., 2007) were taken from literature or estimated so as to best reproduce available data about the time course of IAV infection in a naïve host.

The maximum likelihood (ML) and its special case of least squares estimation is the most common regression scheme that is used for parameter estimation. In ML estimation, the likelihood of a parameter set is equal to the probability of obtaining the available experimental data from a process that is represented by the tested model(Jaqaman et al., 2006). So, the most likely parameter values are computed as the parameters maximizing the probability of observing the experimental data (Jaqaman et al., 2006).

This probability is defined as a function of the differences between the model-predicted data and the experimentally observed data, and it increases as these differences decrease. In our model for the human immune response to IAV infection, it is highly nonlinear making the description of the a posteriori distribution not easy. The two sources of differences between model generated and experimental data are measurement errors and parameter variability. We assume that these differences are not correlated and follow a normal distribution.

Let us represent the model under consideration as a nonlinear map ϕ that to a given set of parameters $\alpha = \{\alpha_1,...,\alpha_p\}$ (in our case the kinetic rate constants) assigns a set of predicted

values $c = \{c_1,...,c_q\}$ corresponding to the available clinical data $d = \{d_1,...,d_q\}$ (for example, the magnitude of viral load at a specified time, maximum value of damage, etc.), i.e., $c = \phi(\alpha)$. The likelihood L of a parameter set α is given by:

$$L(\alpha) = \prod_{j=1}^{q} P(\Delta r_j) \qquad (1)$$

where

$$P(\Delta r_j) = (2\pi\sigma_j^2)^{-\frac{1}{2}} \exp\left(\Delta r_j^2 / (2\sigma_j^2)\right) \qquad (2)$$

is the likelihood of the residual $\Delta r_j = \left\| c_j - d_j \right\|$, representing the model error at the data point j, and σ_j^2 is the variance of the distribution of Δr_j.

The probability $\rho(\alpha)$ of a parameter set α given observed experimental data is obtained from the likelihood function $L(\alpha)$ using Bayesian inference based on *a prior* distribution $\theta(\alpha)$, as follows,

$$\rho(\alpha) = \frac{L(\alpha)\theta(\alpha)}{\int L(\alpha)\theta(\alpha)d\alpha} \qquad (3)$$

where $\int L(\alpha)\theta(\alpha)d\alpha$ is the normalizing constant.

The prior distribution represents our *a priori* knowledge about the ensemble model that is independent of the measured data. *A priori* information tells us what would be the biologically reasonable ranges of parameter values for the biological processes under consideration in the model. The posterior distribution is derived from the degree of fit between the data predicted from models and the observed clinical data and it summarizes the uncertainty on the parameter space. In the present case, the *prior* distribution $\theta(\alpha)$ for each parameter value is determined as the normal distribution whose expectation is the baseline value of the parameter and variance is

taken to be 0.5. Any new parameter value determined based on *a priori* distribution lies in the range of 3-fold higher or 3-fold lower with respect to the baseline value.

3.2.2 Ensemble Model

Consider now a deterministic ODE model $\dot{\mathbf{x}} = \mathbf{f}(\mathbf{x}, \alpha)$ with parameters $\alpha = \{\alpha_1, ..., \alpha_p\}$. The forward problem is the problem of predicting or calculating the "observables" $c = \{c_1, ..., c_q\}$ that constitute the output of the model for given α and can be generally computed from the trajectory $\mathbf{x}(t; \alpha)$ of the model. (Examples of such observables can be the value of a variable at a specified time, the maximum value of a variable over a specified interval, the time t when a specified variable exceeds a specified threshold, and many others.)

The classical problem of model fitting is to find the set of parameters $\alpha^* = \{\alpha_1^*, ..., \alpha_p^*\}$ for which model predictions are closest to observed data $d = \{d_1, ..., d_q\}$ in a precisely defined sense. Because of the lack of sufficient data, experimental uncertainties, or parameter uncertainty (resulting from pooling results from multiple observations together) the values of d are known only to within an error characterized by standard deviations $\sigma = \{\sigma_1, ..., \sigma_q\}$.

The *ensemble model problem* replaces the search for the best model α^* by asking what information can we infer on the model associated with α based on the observations d or, in other words, "what is the distribution of α that represents the likelihood of a particular model capturing the data d". Thus a single value α^* is replaced by a probability density $\rho(\alpha)$ and a single system of ODEs $\dot{\mathbf{x}} = \mathbf{f}(\mathbf{x}, \alpha)$ with fixed values of a parameter set α, is replaced by an ensemble of systems that are identical in their structure (i.e., function $\mathbf{f}$) but differ in the values

49

of system parameters α (see Figure 3-1). Each parameter vector is assigned a weight $L(\alpha)$ that

is proportional to the likelihood with which the available data $d = \{d_1, d_2, ..., d_q\}$, are described

by the trajectory $\mathbf{x}(t; \alpha)$ of the system (see Fig. 3-2). This weight is computed using Equations

(1)-(3) and it represents the model ability to capture clinical observations in which the residual

Δr_j is taken to be the difference between model prediction c_j and data measurement d_j and σ_j^2

is the variance of the uncertainty at d_j.

$$\dot{x} = f(x, \alpha_1)$$
$$\dot{x} = f(x, \alpha_2)$$
$$\dot{x} = f(x, \alpha_3)$$

$$\dot{x} = f(x, \alpha) \quad \longrightarrow$$

$$\dot{x} = f(x, \alpha_n)$$
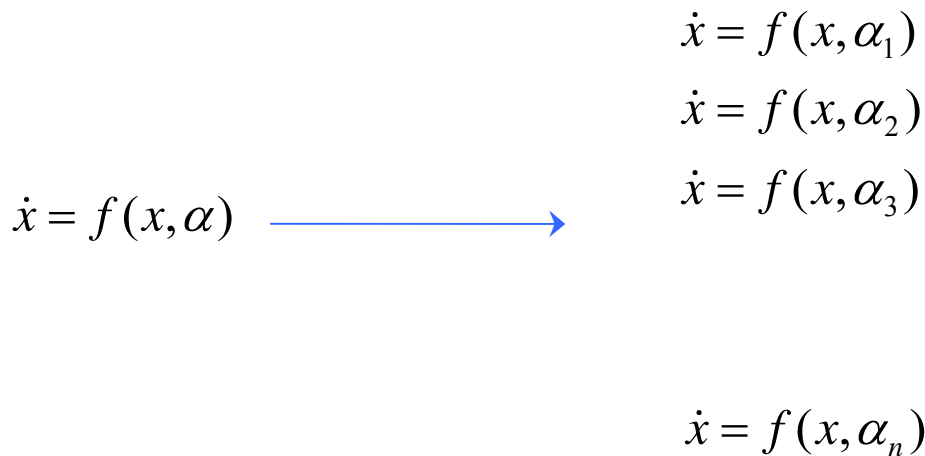
Figure 3-1. Schematic representation of the ensemble model.
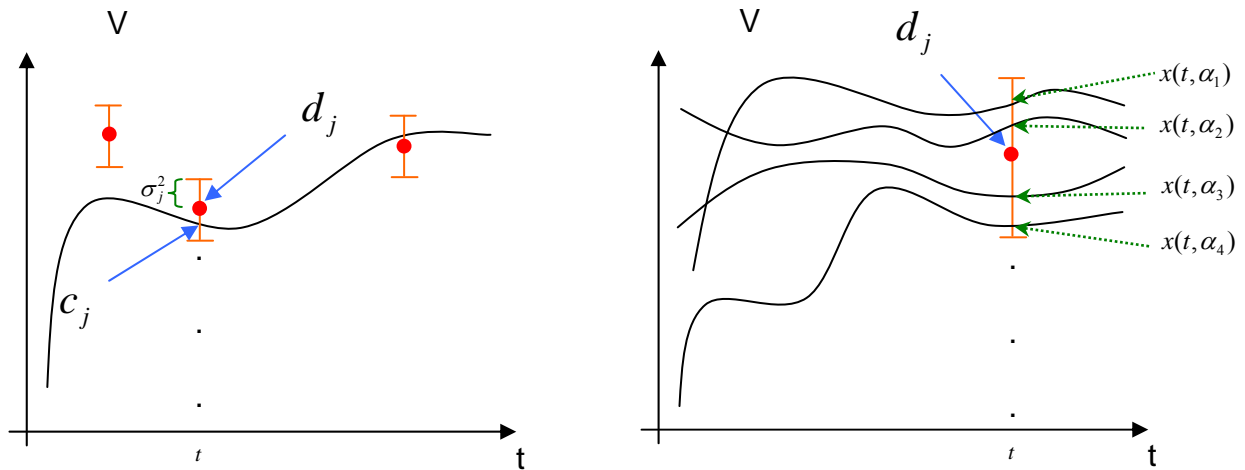
Figure 3-2. Computation of the likelihood function. On the left, a sample trajectory is shown together with data point d_j and the model prediction c_j. On the right, sample trajectories of the distribution are shown.

3.2.3 Metropolis Monte Carlo sampling

The probability density function $\rho(\alpha)$ assigns a value to every point in the accessible region of the parameter space, which generally has many dimensions. One practical way of representing such a distribution is by a random sample of points $\alpha^1,...,\alpha^M$ selected so that the probability of occurrence of α^i in the sample is equal to $\rho(\alpha^i)$. The Metropolis Monte Carlo method (MMC) provides such a sample by utilizing the concept of random walk. "The Monte Carlo method" was first used by Metropolis and Ulam in1949. In 1953, Metropolis introduced the Metropolis algorithm which samples a space according to a Gibbs-Boltzmann distribution. It is a random walk that samples the posterior distribution $\rho(\alpha^i)$ with iterations based on a probabilistic rule. Sampling of the model space is improved by the method given in Wiggins

51

(Wiggins, 1969; Wiggins, 1972) in which the parameter space is sampled according to the prior distribution $\theta(\alpha^i)$.

To illustrate the MMC algorithm on a simple example, let us consider a discrete space S of N states and a Markov chain on the space S given by transition probabilities $\{P_{ij}\}_{i,j=1}^{N}$. The probability that at the step n the chain is at the state i is given by p_i^n. At the next step, the probability will be $p_i^{n+1} = \sum_j P_{ij} p_j^n$. As number of steps goes to infinity, the probability of being in the state i converge to a distribution $\pi_i = \lim_{n \to \infty} p_i^n$ called the "equilibrium probability distribution" (Feller, 1970). If it is possible to go from any point to any other point in the graph with finite number of steps, then there is a unique equilibrium probability distribution π_i for the $\{P_{ij}\}_{i,j=1}^{N}$ independent of the initial probabilities p_i^0 for the process (Feller, 1970).

The goal of the MMC algorithm is to find for a given prescribed distribution $\{\rho_i\}_{i=1}^{N}$ a Markov chain that has a unique limiting distribution $\{\pi_i\}_{i=1}^{N}$ such that $\pi_i = \rho_i$. This Markov chain is found as a random walk in the following way:

1. A random starting point i^1 is chosen.

2. A random step is made from the current point i^n to a new point j according to some fixed proposed transition matrix $\{Q_{ji^n}\}$. (No restrictions are placed on $\{Q_{ji^n}\}$ other than it is a symmetric, doubly stochastic matrix.)

3. The new point j is accepted as the next point in the random walk with the probability $P = \min\{1, \rho_{i^n} / \rho_j\}$. (In other words, if $\rho_{i^n} \geq \rho_j$ then $i^{n+1} = j$, while if $\rho_{i^n} < \rho_j$ then with probability $1 - \rho_{i^n} / \rho_j$ the point j is rejected.)

2nd and 3rd steps of the algorithm are repeated and accepted points $i^1, i^2, ..., i^n, ...$ are stored. The random walk $i^1, i^2, ..., i^n, ...$ generated in this way is guaranteed to have the limiting probability distribution $\{\rho_i\}_{i=1}^{N}$ (Feller, 1970).

A special case of the above algorithm in which we sample Gibbs-Boltzmann distribution $\rho_i = \exp(-\beta E_i)$ corresponding to some energy function E_i is called the Metropolis algorithm.

The implementation for continuous state space is analogous to the discrete space implementation and is described in detail below in Section 3.2.5.

3.2.4   Parallel tempering method

In order to maximize sampling the whole accessible region of the parameter space, we incorporated parallel tempering simulation method into our numerical simulations. Parallel tempering, or replica exchange, is a simulation method to improve the sampling methods of Markov chain Monte Carlo simulations. Replicas of a system of interest were simulated at a series of temperature exchanging the configuration information in a 1986 paper by Swendsen and Wang (Swendsen et al., 1986). The more familiar form of the model originates from Geyer *et al.*(Geyer et al., 1991). First, the method has been applied only to the problems in statistical physics. Since $\beta = (kT)^{-1}$, several replicas of the system are simulated at a series of β values. Replicas at adjacent temperatures exchange partially their configurations through swapping. Configuration swaps between the lower and higher temperature systems allow the lower temperature systems to escape from one region of model space where they could be stuck (at a local minima) and to sample a representative set of another low energy minima(Earl et al., 2005). The highest temperature (lowest β) has to be high enough so that no replicas become stuck in

local energy minima, while the number of replicas used has to be sufficiently large so as to ensure that swapping occurs between all adjacent replicas.

At each Monte Carlo step, the method updates the system by swapping the configuration of the two systems, or trading the two temperatures. The update can be accepted or rejected with the Metropolis rule. This update can be generalized to more than two systems. By carefully choosing the β values (temperatures) and systems, significant improvement in the mixing properties of several Monte Carlo simulations can be achieved that exceeds the extra computational cost of running parallel simulations.

The systems associated with higher temperatures are able to sample larger volumes of the parameter space, whereas the ones associated with lower temperatures make precise sampling in a local region of the model space. The ones with lower temperatures may become trapped in a local minima staying there and sampling around it for a longer period of time in computer simulations. Parallel tempering method promotes mixing of random walks in parameter space and hence enhances sampling of local minima. During the process, lower temperature systems make small jumps in the neighborhood achieving complete sampling around local minima, whereas the higher ones make bigger jumps scanning the whole parameter space finding different local minima in the model space. Therefore, we not only gain access to all possible local minima in the model space but also achieve good sampling around them. All the information inferred using replicas at different temperatures are stored in a single replica from which we obtain a posteriori distribution. In our simulations, this single replica corresponds to the one for which the β is equal to 1.

Simulation of 5 replicas rather than one requires on the order of 5 times more computational time. Because of enhanced mixing properties, it is more efficient to have the

original single-temperature Monte Carlo simulation run 5 times longer. Different replicas can also be run in parallel as an extra benefit of this method. Figure 3-3 shows how quickly the parallel tempering method reaches equilibrium and how average energies of random walks at different values of β are inversely proportional to β, which allows the chain with the lowest β to sample larger regions of the space. Figure 3-4 shows the histogram of the parameters γ_{VA} and α_V. γ_{VA} is the rate constant of neutralization of IAV by antibodies and α_V is the rate constant of nonspecific IAV removal. Both are important parameters for the disease dynamics as described in Table 2-2. Figure 3-5 shows an example of how mixing is enabled by swapping chains with different β. In the figure, swaps are visible as jumps between distant values of each parameter.
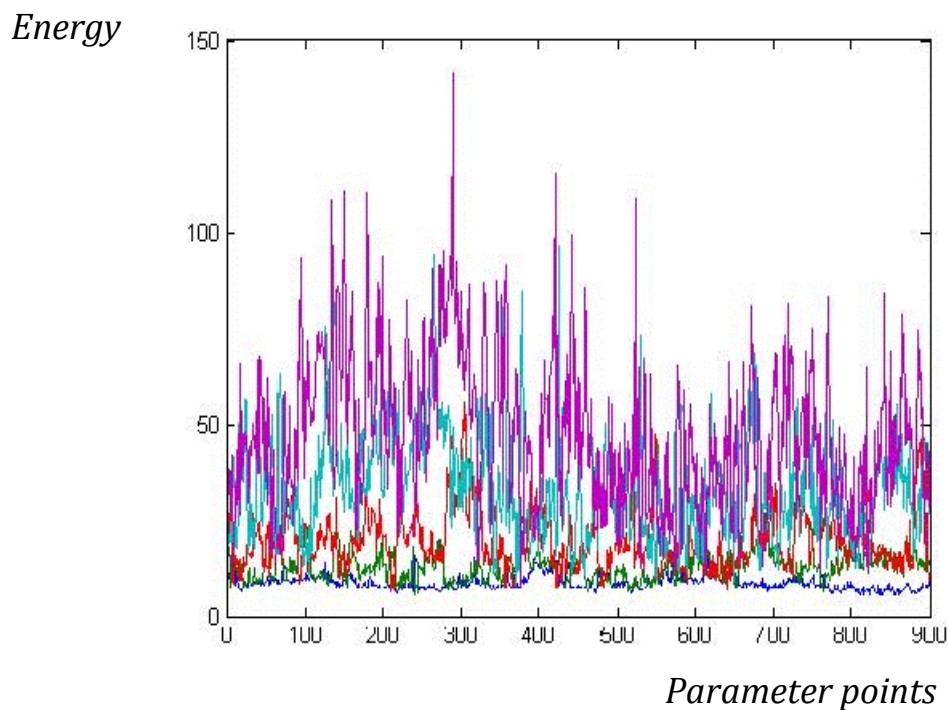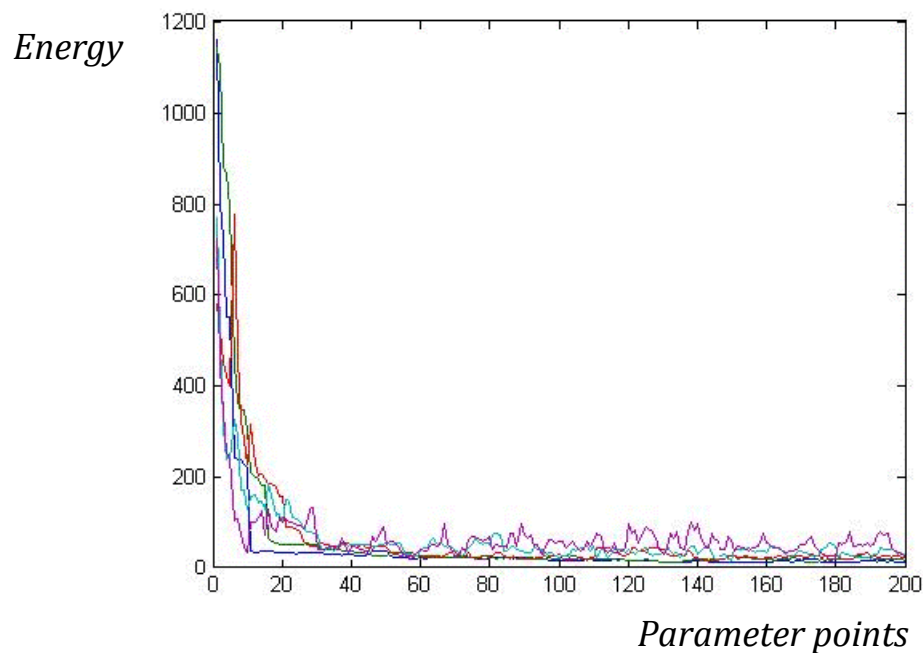
Figure 3-3. Convergence and equilibration of the parallel tempering Monte Carlo algorithm. The energy for each of the 5 replicas of random walk generated by MCM algorithm associated with different values of β : 1 (blue), 0.5 (green), 0.25 (red), 0.125 (cyan), and 0.0875 (magenta). Examples of an initial part of a run (above) which represents the first 200 points in the sample and equilibrated portion (below) which represents the last 900 points are shown.
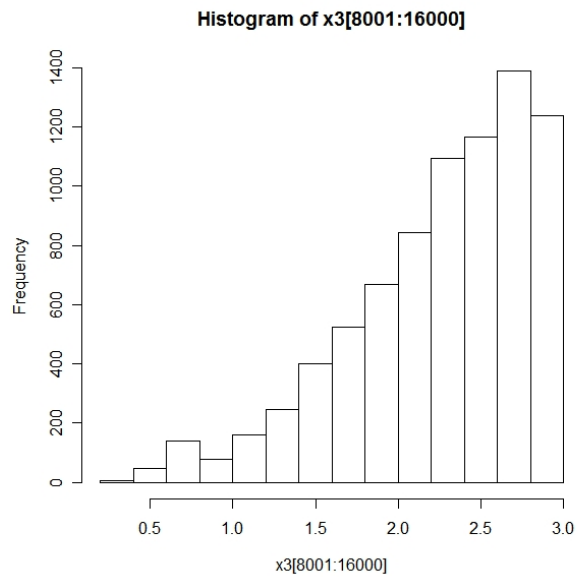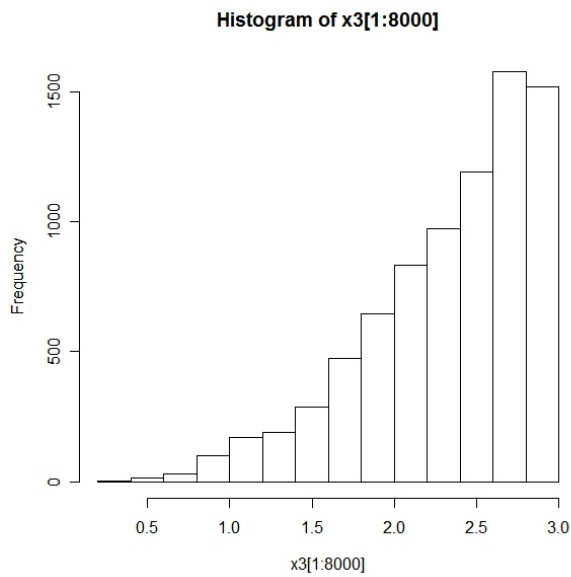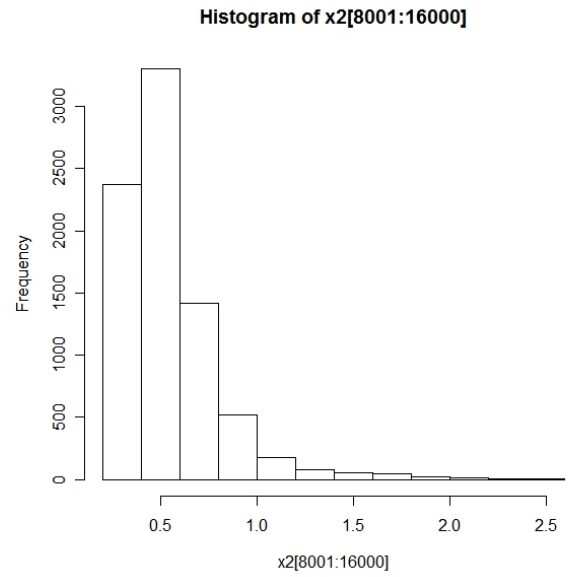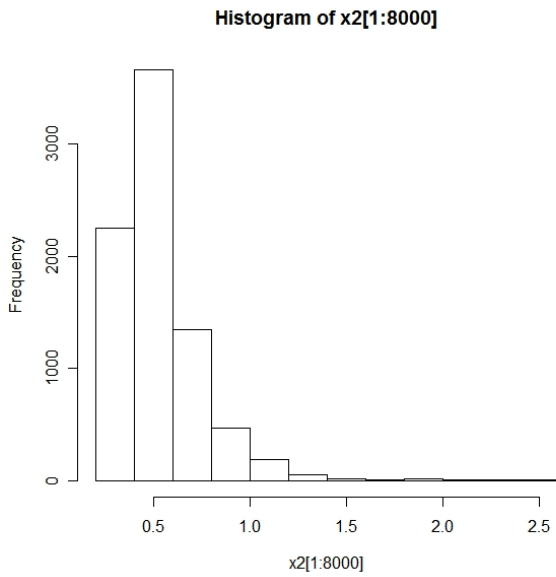
Figure 3-4: Histograms of the parameters γ_{VA} (above) and α_V (below) are shown for the first part of the chain (on the left) and the second part(on the right). The similar pattern of the histograms of parameters at different parts of the chain indicates the convergence to the posterior distribution. The y axes shows the frequency of parameters over the parameter space and the x axes indicates the parameter values; 1 is the baseline value and possible parameter values lie between 1/3-3(3-fold less and 3-fld high).

Parameter values

Around the baseline
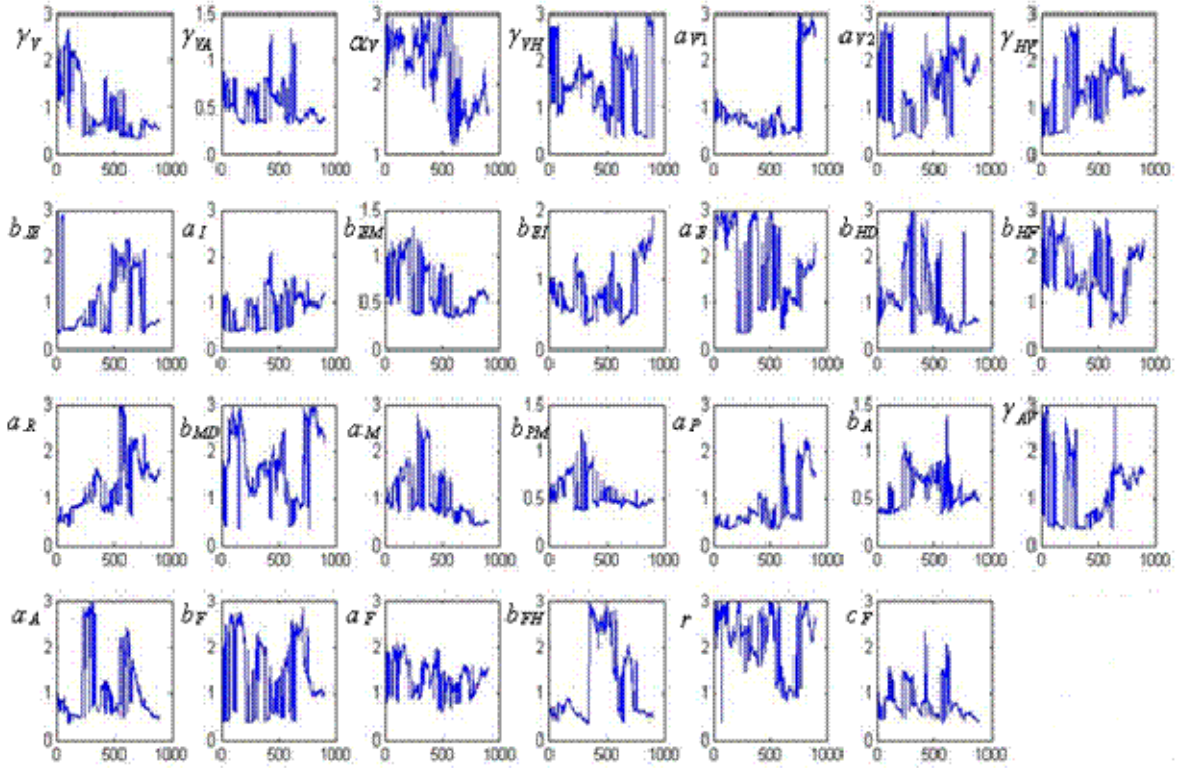
Parameter points

Figure 3-5. Examples of the variation of values of all 27 parameters along the random walk for replica with $\beta = 1$.

3.2.5 Implementation of Metropolis Algorithm to the Influenza Modeling

We are interested in finding a posterior distribution $\rho(\alpha)$ over the 27 dimensional parameter space of the deterministic ODE model described in Chapter 2 using the equations (1)-(11). The distribution $\rho(\alpha)$, defined by equations (1)-(3) of Section 3.2.1 gives the complete solution of the inverse problem and describes all the information we have on the system. To

represent $\rho(\alpha)$ in the computer simulations, we will sample the points according to Metropolis Algorithm from the accessible region of the parameter space. Each point α in the parameter space represents a parameter vector with 27 components:

$$\alpha = \{\alpha_1, \alpha_2, ..., \alpha_{27}\}$$

The total data set d to fit the model contains 13 data points described in the subsection **3.2.6**:

$$d = \{d_1, d_2, ..., d_{13}\}$$

Briefly, 7 of these data points are taken from the time courses of the virus titers in 19 human volunteers as reported in (Hayden et al., 1998) and the other 6 points are chosen to be the maximum levels that *D, E, P, S, A* and *F* variables could achieve during the course of infection as given in Bocharov *et al.* The values $d_1, d_2, ..., d_{13}$ are the expected values of the time courses of model variables at points where the data is available. The standard deviations $\sigma = \{\sigma_1, \sigma_2, ..., \sigma_{16}\}$ for the virus data are taken from (Hayden et al., 1998) while they are chosen according to the expected qualitative model behavior for other 6 points. We could add more data points to fit or set the standard deviations more accurately with the availability of broader clinical data. This would give more assurance for the posterior density we get. However, the essence of the method that we describe would not change.

We sample the points in parameter space starting from the default parameter set which consists of the baseline parameter values for the model in (Hancioglu et al., 2007). We could start the sampling algorithm from any point randomly chosen in the accessible region. A sample $\alpha^1, ..., \alpha^M$ representing the probability distribution $\rho(\alpha)$ is found according to the Metropolis Algorithm as described in the subsection **3.2.3**.

1. A starting point α^1 is taken to be the default parameter set.

   For a current state α^n we compute E^n, the energy at the point α^n, as $E^n = -\ln \rho(\alpha^n)$.

2. A new set of parameters $\bar{\alpha}$ is generated according to the proposal density Q which is taken to be a Gaussian probability density with variance ε centered at the current point α^n, i.e., $Q(\bar{\alpha}) = (2\pi\varepsilon)^{-1/2} \exp\left(-(\bar{\alpha} - \alpha^n)^2 / (2\varepsilon)\right)$. If any parameter value in the new set $\bar{\alpha}$ is above 3-times the default or below one third the default, that value is rescaled to fit within these limits.

3. $\bar{E}$, the energy of the new state is computed as $\bar{E} = -\ln \rho(\bar{\alpha})$

4. If $\bar{E} \leq E^n$ then $\bar{\alpha}$ is accepted as the new point, i.e., $\alpha^{n+1} = \bar{\alpha}$, and the algorithm goes back to Step 2. If $\bar{E} > E^n$ then $\bar{\alpha}$ is accepted, i.e., $\alpha^{n+1} = \bar{\alpha}$, with probability $P = \exp\left(-\beta(\bar{E} - E^n)\right)$, otherwise it is rejected, i.e., α^{n+1} is not assigned. The algorithm then goes back to Step 2.

The algorithm keeps track of the acceptance ratio of the proposed parameter sets, i.e., the ratio of accepted to total proposed new sets. Optimal convergence is achieved if the acceptance ratio is around 0.4(Feller, 1970). The acceptance ratio increases with decreasing values of β and ε. In other words, the acceptance increases if we lower the multiplier β which will make energy increases more acceptable, or if we make smaller jumps. In the present case, $\beta = 1$ is fixed and $\varepsilon = 0.01$ was found to be optimal by trial and error.

Metropolis algorithm samples the points $\{\alpha^1, \alpha^2, ... \alpha^M\}$ in the parameter space where each new point is sampled according to the posterior distribution.

$$\alpha^n \longrightarrow E^n \xrightarrow{\varrho(\alpha)} \bar{\alpha} \longrightarrow \bar{E} \xrightarrow{\text{Metropolis rule}}$$

Accepted: $\alpha^{n+1} = \bar{\alpha} \longrightarrow E^{n+1} \xrightarrow{\varrho(\alpha)} \bar{\alpha}$

Rejected: α^{n+1} is not assigned

$\bar{\alpha}$
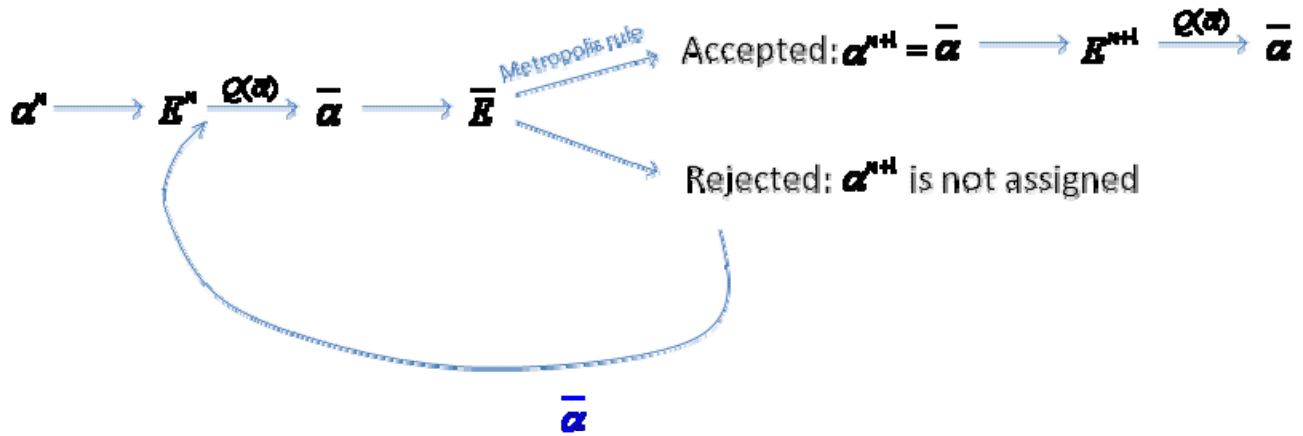
Figure 3-6. Schematic representation of the Metropolis sampling algorithm.

 The classical MMC method may get stuck at a local minimum or a particular region in the parameter space. The modeler needs to get around this problem. One way of rescuing from the region where the convergence is no longer good and making sure that the sampling algorithm samples all over the accessible region of the parameter space with sufficient number of iterations is to apply the ***Parallel Tempering method*** as follows: We simulated 5 replicas of the original system, each with a different value of β_i such that $\beta_1 > \beta_2 > ... > \beta_5$. $\beta_1, \beta_2, \beta_3, \beta_4, \beta_5$ are chosen to be 1, 0.5, 0.25, 0.125, 0.0675, respectively. The value of ε has been determined by trial and error to satisfy the acceptance ratio of 0.35 for each replica. $\varepsilon_1, \varepsilon_2, \varepsilon_3, \varepsilon_4, \varepsilon_5$ are determined to be 0.023, 0.035, 0.053, 0.08, 0.12 respectively to satisfy this acceptance ratio. Therefore, replica #5 could make bigger jumps than other replicas and in case the process becomes stuck at a certain region in the parameter space, it would rescue the process by jumping another region. Each replica uses the Metropolis algorithm to produce a random walk with the limiting probability distribution $\rho_i(\alpha) = \exp(-\beta_i E(\alpha))$. At each step, n swaps are attempted between replicas with

adjacent   values   of β with   the   probability

$$P = \min\{1, \exp((\beta_i - \beta_j)(E_i^n - E_j^n))\}$$

Let $\alpha_1^n, \alpha_2^n, \alpha_3^n, \alpha_4^n, \alpha_5^n$ represents the sample of parameter sets for each replica at the

step n. i.e. α_i^n are the points sampled by the chain with $\beta = \beta_i$. Through swapping occurred with

other chains, this chain would sample the whole accessible parameter space and provide us the

unique posteriori distribution. The following figure illustrates swapping between the 1st and 2nd

replicas:
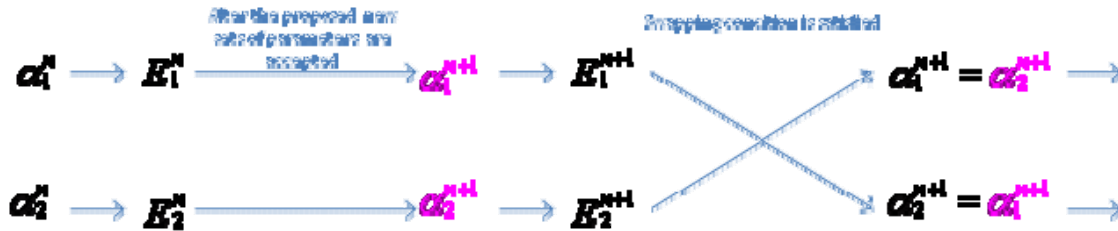
Figure 3-7. Schematic representation of swapping between the replicas.

3.2.6   Simulations

We used MATLAB 7.0 to run all simulations. The ensemble models are obtained by

numerical integrations of ODEs using the MATLAB stiff solver, ode23s. The parameter set

associated with previously published model is taken as a starting point for the Metropolis

algorithm & parallel tempering method even though random starting point would be sufficient

for the algorithm. The parameter values in this set are close to those in (Bocharov et al., 1994)

yet rescaled to dimensionless quantities. Acceptance ratio of new points in the replicas was about

0.35 which is considered very efficient for the algorithm. Energy calculation or likelihood of a specific model is computed based on the following available clinical data and set of observations considering the response of a naïve host to the standard initial conditions (see below) (Bocharov et al., 1994)& (Hancioglu et al., 2007): (i) Time courses of virus titers after experimental influenza A/Texas/36/91(H1N1) are taken from (Hayden et al., 1998). Standard deviation of each data point is calculated from the information given in (Hayden et al., 1998). (ii) Effector cells E peak with approximately 10^2 fold increase over the homeostatic level. Standard deviation of peak E value is set to 0.5 (on logarithmic scale) (iii) P cells peak at 10^4 fold level. Standard deviation of P at the peak is set to 0.5 (on logarithmic scale) (iv) After 15 days, the compatibility S is 0.8. Standard deviation of S at the peak is set to 0.1 (v) Maximum level of dead cells D_{max} is 35%, i.e., 0.35. Standard deviation of D at the peak is set to 0.2 (vi) Interferons F peak at 10^4 fold level and after 2 days of the infection. Standard deviation of the time of peak for F is set to 0.5 (on logarithmic scale) (vii) Antibodies A peak at 10^3 fold level. Standard deviation of A at the peak is set to 0.5 (on logarithmic scale).

3.3   RESULTS

3.3.1   Standard behavior

The standard behavior for ensemble models describes probabilistic prediction of the course of infection in a naïve host. We assume that initially the host has no dead, infected or resistant cells, no interferon molecules, and no activated APC (i.e., H(0) = 1, I(0) = M(0) = F(0) = R(0) = 0). The initial levels of effectors, plasma cells, and antibodies are assumed to be at the

63

homeostatic values (i.e., $E(0) = P(0) = A(0) = 1$) (Asquith et al., 2003). In a naïve host, we assume that $S(0) = 0.07$ which corresponds to a relatively low compatibility with the virus strain, that may have resulted from previous exposure to IAV and subsequent genetic drift. In the typical course of acute IAV infection, the initial concentration of aerosol delivered virus particles that the host receives is about 10^5 particles per ml on day 0, corresponding to $V(0) = 0.001$ in our dimensionless system. The initial values are assumed fixed over the entire ensemble of parameter values. The resulting probabilistic prediction of time courses of model variables corresponding to naïve infection are depicted in Figure 3-8.
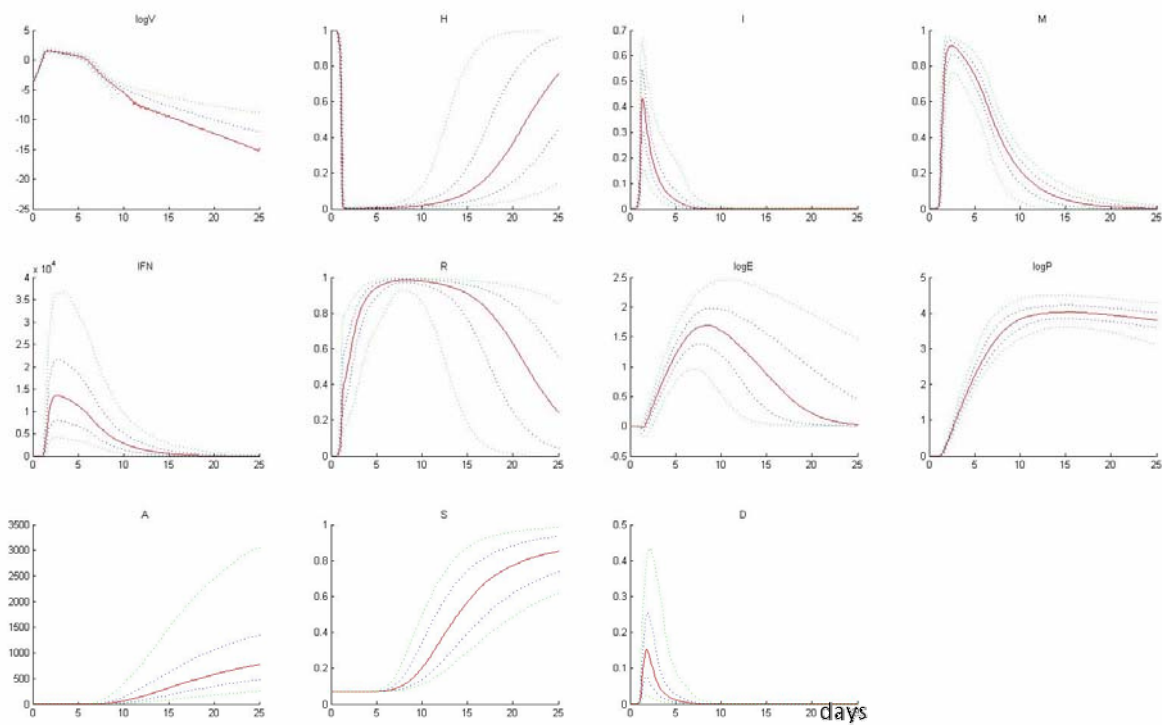
Figure 3-8. Statistical analysis of trajectories of the ensemble model showing, for each variable, the following percentile levels as a function of time: 5th percentile (lower green dots) , 25th (lower blue dots), 50th (black curve), 75th (upper blue dots) and 95th (upper green dots). Only trajectories with single peak in V have been selected.

As seen in Figure 3-8, virus level peaks (period of maximum antigen concentration) after 2 days for almost all trajectories. (In Chapter 1, we showed that the onset of disease depends on initial viral load; the larger the V(0), the sooner the onset of disease.) Peak viral load is increased by 10^4 fold with respect to initial value for the big majority of models staying at peak approximately 3 days, in accord with experimental data (Tamura et al., 1998). Viral load starts to decline to inoculation level after day 5 (early stage of recovery, disappearance of IAV particles) and are removed from the system completely within 15-20 days in 98% of the cases. As we mentioned above, in 2% of cases viral titers are rebounded after about a week peaking at variable days depending on the model (from day 8 to 17) although the majority peaks at day 13. The host is considered infectious when the virus level exceeds 1, which happens after day 1 for almost all individuals. The host remains infectious for about 2.6 days. APC are activated after 1 days peaking after about 3 days and returning to homeostatic levels within 8-10 days. Although the virus titer trajectory is essentially identical for all parameter sets, the amount of healthy cells at day 15 varies widely over the ensemble distribution. While 50% of cases remain with H below 0.2 (and hence majority of epithelial cells are resistant), 5% of cases show essentially full recovery to H = 0.9. It is not until day 22 that 50% of cases are halfway through complete recovery of healthy cells.

The resulting loss of respiratory epithelial cells (dead cells) is one major reason for several of the symptoms that accompany infection, such as cough, depressed tracheobronchial clearance, and altered pulmonary function (Hayden et al., 1998). We consider the host "symptomatic" if the damage level exceeds 10% of the epithelial cells(Marchuk et al., 1986), which occurs when the viral load peak at day 2. The maximum proportion of dead cells is varied through the population starting from insignificant levels to 40% mostly attained between days 2

and 3. 25% of the population is considered asymptomatic whereas 5% of them suffer from severe symptoms and a little more than half of people follow the regular flu trajectory. The symptomatic period is between 2 to 4 days after which time most of the cells become resistant to the infection. Infected cells reach a maximum proportion of 15-55% of all cells after day 2 for above 90% of the population, while the proportion of resistant cells peak after 5-10 days based on individual, which is in accord with the experimental observation that the expression of nucleoprotein (NP) mRNA in epithelial cells, showing the presence of infected cells, changes in parallel with viral titer (Tamura et al., 2004). By the action of the innate immune response, almost everybody becomes resistant to infection for the standard case when R reaches levels of 90% and above at the peak.

Interferon response comes into play once the virus peaks at day 2 making most of the cells resistant to infection. Interferon level is increased by $10^1 - 10^2$ folds for more than half of the population peaking approximately at day 3. It reaches levels of up to the 10^4 fold increase for some of the individuals. Plasma cells are produced after 2-3 days before virus-specific antibodies are detectable peaking between days 10 and 15, in accord with empirical observations (Ada et al., 1986). Antibody production by plasma cells begins at day 8. The amount of antibody increase falls in a big range averaging 10^3 fold in the population when the adaptive immune response comes into play to remove all viral particles and generate immune memory. Furthermore, antigenic compatibility is increasing monotonically starting right after when the adaptive immunity is activated (after day 8) and the antibodies are capable of inhibiting viral particles with 80% probability in median after 15 day of infection. When the infection is over, specific antibody levels of the population is ranging between 60-100% to the subtype.

For about 2% of all the trajectories, the curve of viral titer versus time has two peaks within 20 days. When we continue simulations after 20 days, we still observe rebound of trajectories showing chronic behavior. This bimodal behavior most likely caused by reduction in the production of plasma cells, as they are produced 100 times less on average. These trajectories are shown as rebounded in Figure 3-9.
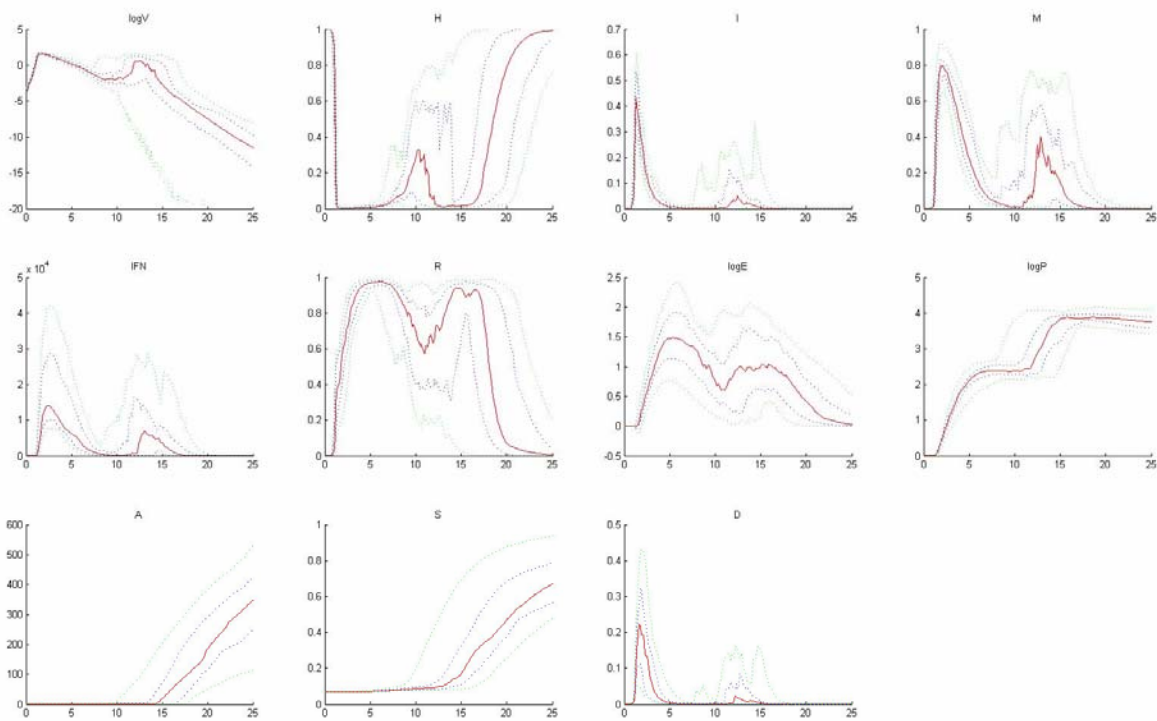
Figure 3-9. Statistical analysis of trajectories of the ensemble model for rebounding trajectories with two or more peaks in V.

3.3.2   Superspreaders

Influenza outbreaks cannot be completely understood if individual variation in infectiousness is ignored. Epidemiologists believe that the 20/80 rule applies in most of the infectious diseases, 20% of infected individuals provide 80% of subsequent infections(Woolhouse et al., 1997). Many people don't infect anyone else but a few people, "superspreaders", who come into contact with large number of people, may potentially infect tens or hundreds of people in epidemics. What determines whether an infection dies out or survives is the emergence of these superspreaders. So, public health programs must target this 20% of the population in order to be successful. This requires a better understanding of factors determining individual infectiousness. If highly infectious individuals can be identified effectively then the efficiency of control can be greatly increased. Applying half of the control measures on the most infectious 20% of cases is about 3-fold more effective than random control(Lloyd-Smith et al., 2005). Disease control interventions such as quarantine or isolation of certain individuals and reduction in the number of contacts of infected people could change the infectiousness of an individual.
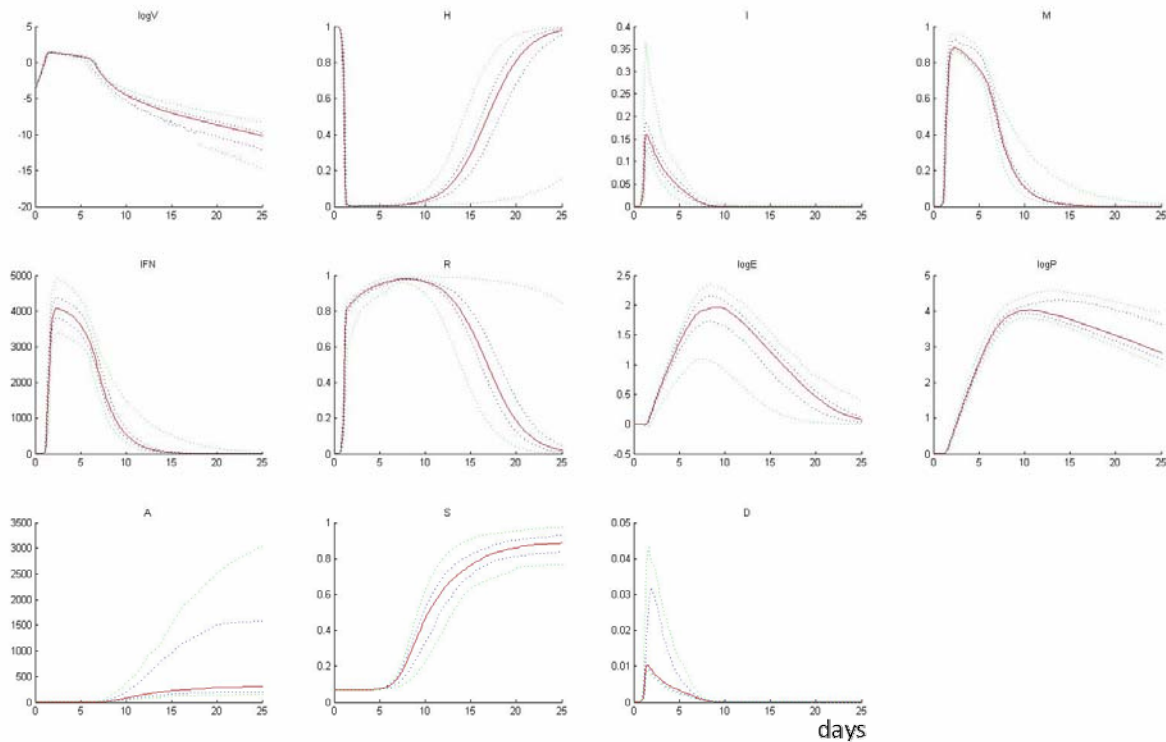
Figure 3-10. Statistical analysis of trajectories of the ensemble model for superspreaders, i.e., individuals with low damage and immune response.

From the several factors that might make someone a superspreader, we consider those individuals who choose not to seek treatment due to low levels of symptoms such as cough or fever and the ones who are immunocompromised. So, in our analysis, this corresponds to low levels of D ($D<0.1$), F ($F<5000$), and sufficient amount of virus shedding ($\log V>1$) at the peak.

The superspreader trajectories account for 0.6 % of all the trajectories of the ensemble model. As we can see from the time courses of percentiles of superspreaders in Figure 3-10, D peaks at the same day with levels less than 10 times for the median of typical trajectories. Proportion of infected cells is decreased by 2-3 times. Activated *APC, P* and *E* are about the same whereas F is decreased by 5-10 times depending on percentiles. In spite of the low level of interferon and damage factor indicating asymptomatic regime, virus load reaches the level of typical disease trajectories. Therefore, although these individuals will not seek treatment just

69

because they feel good, they might be very dangerous in an epidemic since they will interact with others at work, school or in other public places and spread the disease.

3.3.3   Drug therapy

Several treatment scenarios can be considered to determine optimal interventions (vaccination, antiviral drugs, etc.) and effectiveness of therapy for individuals at various conditions (immune, not immune, immunosupressed, etc.). The ensemble model that we constructed is used to make probabilistic predictions of success of selected therapeutic interventions. Using the methods we presented, one can address several questions such as

1. How long and how intense should antiviral treatment be?

2. What is the probability that a value of a given model variable drops below a prescribed threshold at a certain time? (Such as, for example, what is the probability that V drops below 10 (i.e. host becomes noninfectious) at day 3.)

3. How the onset, severity, duration of disease and the contagious period of an individual are changed according to the treatment?

4. What are the effectiveness of various antiviral drugs (HA inhibitors vs. NA inhibitors)

5. When the pathogen is more virulent how the above results are affected?

We can continue on similar questions and one can address all these questions using the posteriori distribution that we computed in the parameter space. Below, we chose to analyze the following question: *Assuming that the length of the treatment is fixed, what would be the optimal time to start the treatment?* We investigate the optimal time to start the treatment to reduce the proportion of people becoming sick, the damage (symptoms), the infectiousness of a person and the duration of infection once the susceptible person is

70

infected. The output of the treatment depends on several factors including the strength of the virus, the strength of immune compatibility of the patient, and the effectiveness of the drug. Here "treatment" refers to administration of drugs which are *NA* inhibitors reducing the replication rate of viruses from infected cells. Duration of treatment is fixed as one week. "Less effective drug" refers to either lower dosages of an effective drug or a drug which reduces the replication rate mildly, i.e., replication rate becomes 3 times lower with respect to the baseline value after the drug therapy. On the other hand, "High effective drug" refers to higher dosages of a drug or the one which reduces the replication rate aggressively, i.e., replication rate becomes 10 times lower with respect to the baseline value after the drug therapy.

3.3.3.1 Effect of therapy for regular flu

Using the posterior distribution over the parameter space, the ensemble model provides the following observations on the course of disease caused by mild-type seasonal influenza A viruses and the effectiveness of antiviral drug therapy:

a) no treatment

Without antiviral drug therapy, when a population is infected by the mild type IAV, the onset of disease is prolonged for those who have higher initial immune status (see Figure 3-11). In this figure, Vtmin is the onset of the disease, i.e. the time when virus titer first crosses the threshold V=1. Vtdur is the duration of the disease, i.e. the time interval between the onset and the last time point at which V crosses below V=1. logVmax is the maximum virus titer in the logarithmic scale. Ftmin and Ftdur are analogous to Vtmin and Vtdur for interferon. Dmax is the maximum damage. Immune individuals have lower level of infectiousness and systemic symptoms. So, either vaccination or early exposure to the same subtype of the virus helps reduce

71

the spread of disease, the severity of symptoms and the transmission. The duration of disease is slightly decreased by increased immunity. For a naïve population, 75% of the population is expected to be sick, instead, only 20% or less people are symptomatic in the immune population. So, probability of becoming sick is increased significantly by being naïve to the infection.

a)

b)

c)

d)
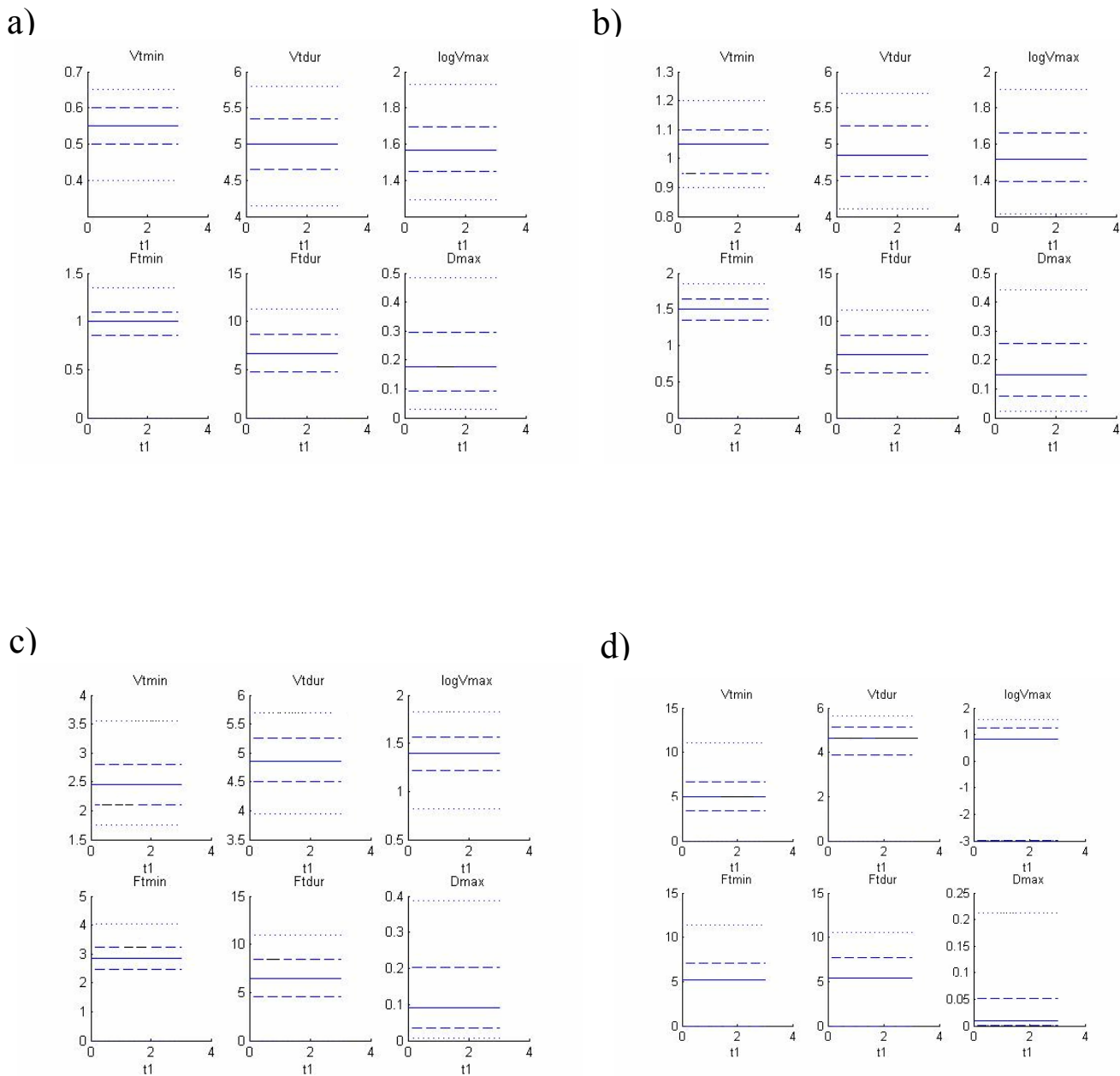
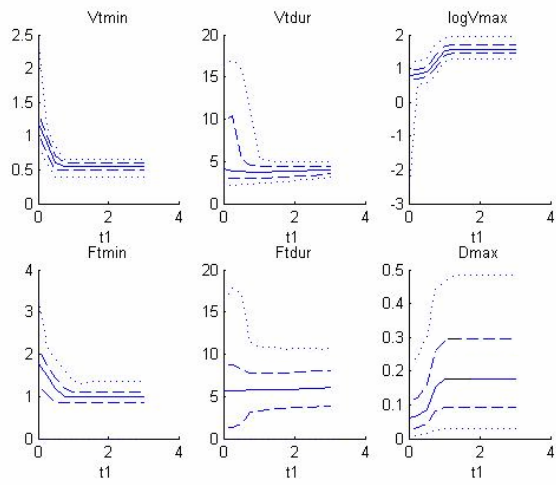**Figure 3-11. Immune response to regular flu for no treatment and different initial antigenic compatibility. a) S(0)=0 b)S(0)=0.07 c)S(0)=0.2 d)S(0)=0.4. Here as in Figure 3-5,6,7 statistics over the distribution of parameters is shown using percentile levels. 5th percentile (lower dots) , 25th (lower dashes), 50th (line), 75th (upper dashes) and 95th (upper dots).**

b) Treatment of regular IAV by low or high effective drug

Type of treatment (drug efficiency & dosage) has significant impact on the onset of infection. The higher the dosage, the more the onset is prolonged. In most of the cases where the host is sufficiently immune to the infection, no disease is expected. The therapy in general lowers the infectiousness of a person. The rate of reduction depends on the initial immune state of the host. For those of without immunity, the high efficient drug administered after about half a day provides a better result. For the ones who have weak immune response, the less efficient drug administered at the beginning of the infection performs the best. For all of the immune people, the treatment heals the infection. The duration of contagious period and the duration of systemic symptoms are not affected by the type of treatment. The infectiousness of a person is decreased after the treatment and the amount of reduction in contagiousness is the same regardless of the dosage and the efficiency of drug. The more effective the drug, the more people will escape from the disease. 25% of people are more likely to be sick after normal drug therapy instead of only 5% is expected to be sick after highly efficient therapy (in a naïve population). For weakly immune individuals ($S(0)=0.07$), these ratios are 5% and 25% respectively. So, higher dosages actually make the case worse. Low dosage or low efficient drug given at the beginning of infection is preferable. For immune population, effect of various dosages is similar.
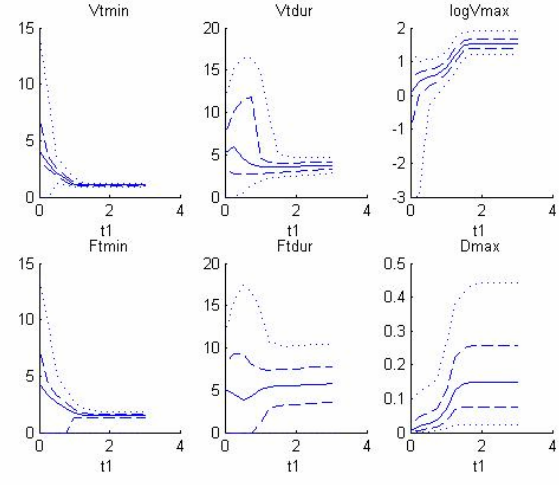
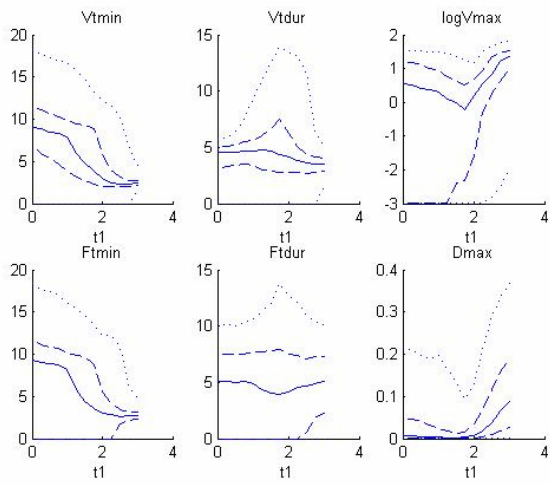**Figure 3-12. Immune response to regular flu treated with low efficiency antiviral drug administered starting at time t1 for 7 days. a) S(0)=0 b)S(0)=0.07 c)S(0)=0.2 d)S(0)=0.4.**

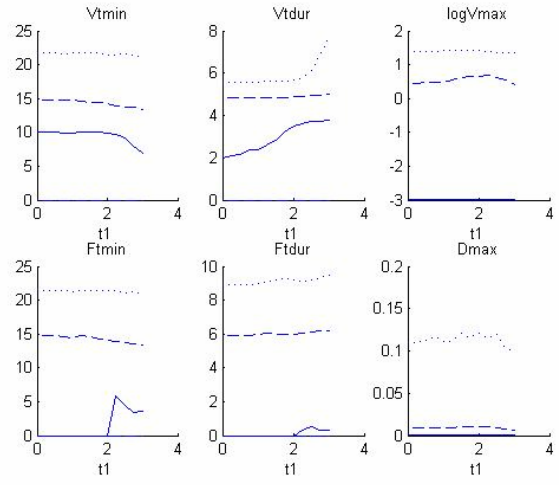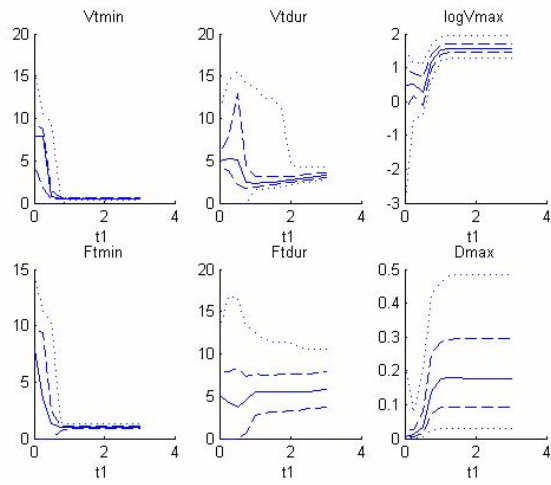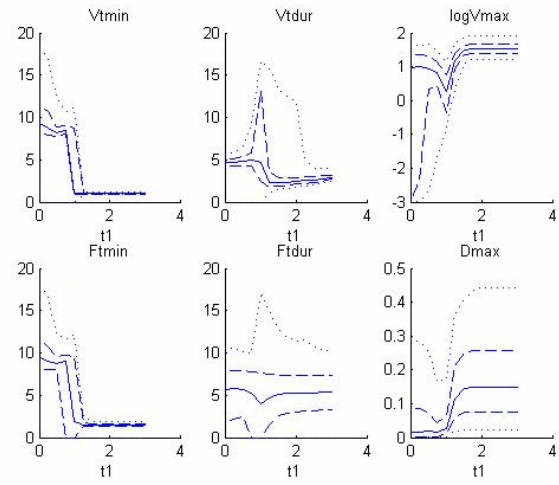**Figure 3-13. Immune response to regular flu treated with high efficiency antiviral drug administered starting at time t1 for 7 days. a) S(0)=0 b)S(0)=0.07 c)S(0)=0.2 d)S(0)=0.4.**

3.3.3.2 Effect of therapy for highly virulent virus

"Highly virulent virus" means the one which is able to infect healthy cells at much higher rate (3 times greater in our simulations). Based on our simulations, the following observations are worth mentioning for the course of disease caused by virulent IAV and for the effect of antiviral drug therapy:

a) No treatment

When antiviral drugs are not used in a population infected by high virulent IAV, the onset of disease is prolonged proportional to the initial immunity of an individual. Other disease characteristics such as duration, infectiousness, severity of symptoms has not been changed significantly depending on the S(0), initial immune state of the host. So, vaccination will not benefit the whole population against a highly virulent virus and unless taking the proper antiviral drug therapy, the population would suffer from the disease with severe symptoms, even with high mortality rates coming along with high transmission rates. Duration of disease is slightly decreased by increased immunity too. For naïve population, 95% of the population is expected to be sick caused by such an epidemic. Timing and dosage of the drug therapy is crucial in this case and affects the onset, symptoms and infectiousness in various ways as explained below:

a)
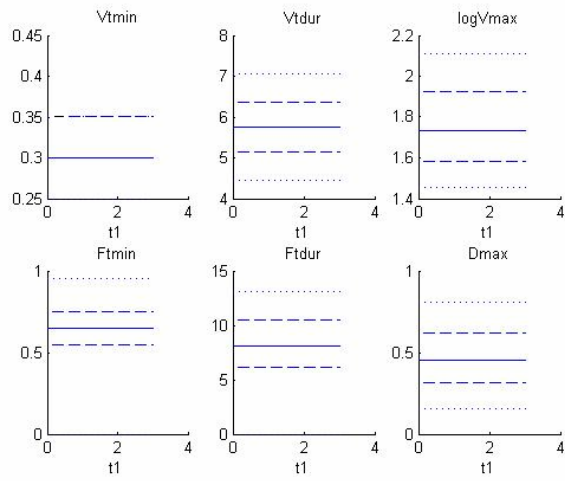
b)
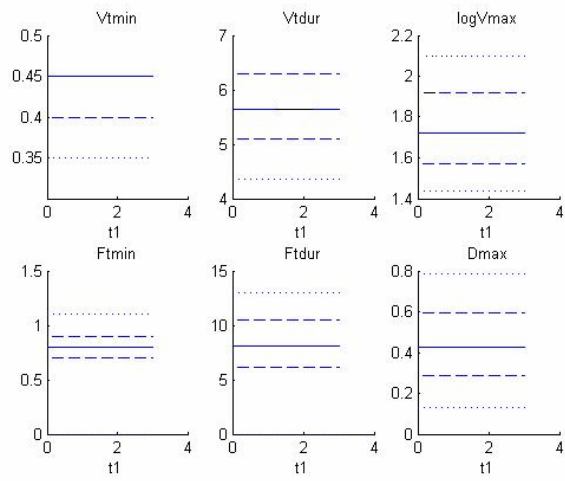
c)
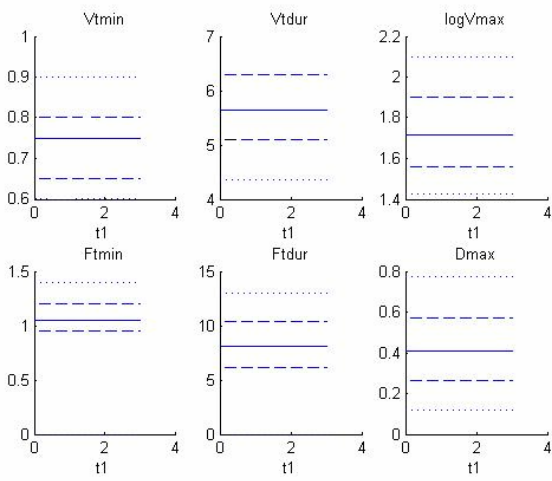
d)
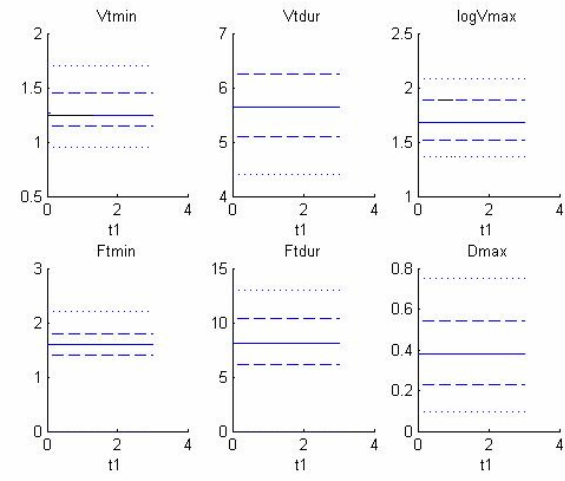
Figure 3-14. Immune response to virulent flu for no treatment and different initial antigenic compatibility. a) S(0)=0 b)S(0)=0.07 c)S(0)=0.2 d)S(0)=0.4

b) Treatment of virulent IAV by low or high effective drug

High dosage prolong the onset significantly; the more effective the drug, the more prolonged the onset of disease. Treatment lowers the contagious period about the same for low and high dosages. Also in this case, therapy lowers the infectiousness of a person. For less effective drug, treatment should start as soon as possible to reduce the infectiousness. For high effective one, optimal time to start treatment depends on the immune status of the host; for naïve host, it is after 6 hours, whereas, for immune individuals, it might be as late as 1 day. So, even unintuitive, optimal time to start treatment is not right after infection for an immune population, it would just make the transmission rates higher in an epidemic.

Drug therapy helps reducing the duration of disease and symptoms. The more effective the drug, the more reduced the duration and optimal time to start is at day 0, right after infection. As expected, the more effective the drug, the more lowered the symptoms. Optimal starting time of treatment to reduce symptoms varies depending on the immune status of the host. Starting earlier is always better whenever low dosages are chosen. When high effective drug is chosen, it should be given to naïve patients after 6 hours, although 1 day is the optimal time to start for immune ones. Giving it at day 0 would not decrease the symptoms as much as when it is given at the optimal time.

The more effective the drug, the more people will escape from the disease for virulent virus as well. However, percentage of people who will be sick in an epidemic is significantly increased due to high virulent strain of IAV. For example, in a naïve population, 95% of the population is predicted to be sick even after low efficient drug therapy whereas 25% of people will be affected by disease when given high effective dosages. 45-50% of relatively immune individuals will develop symptoms even after high efficient treatment. For weakly immune
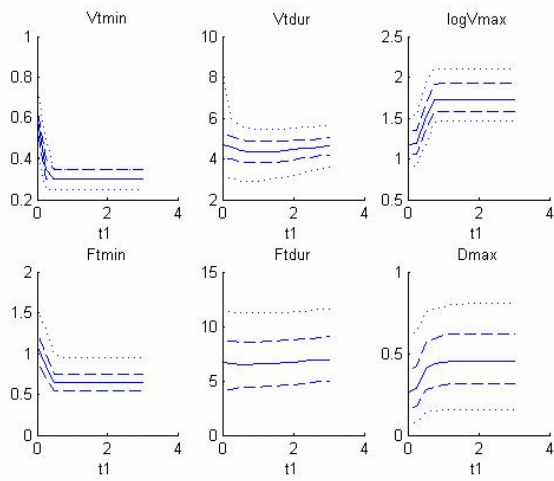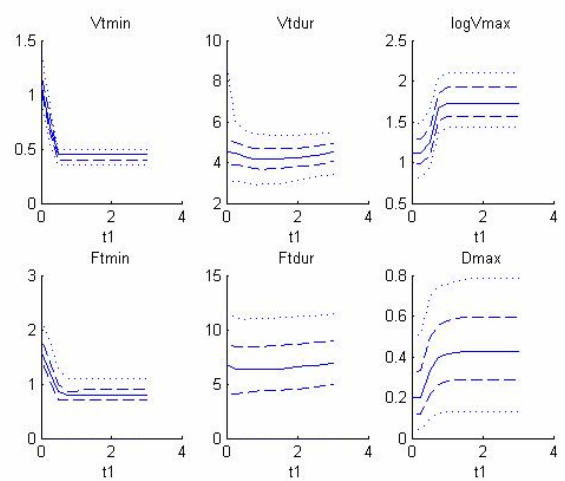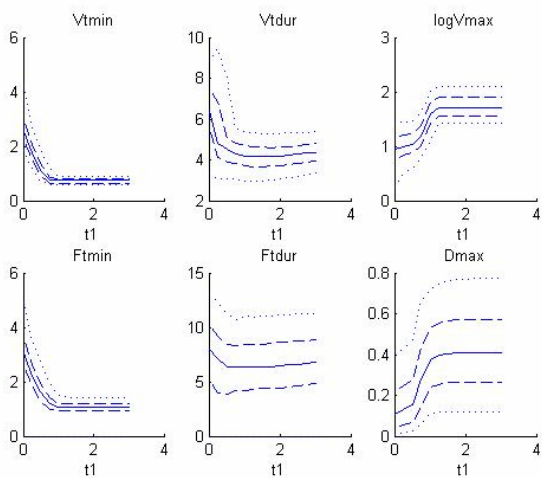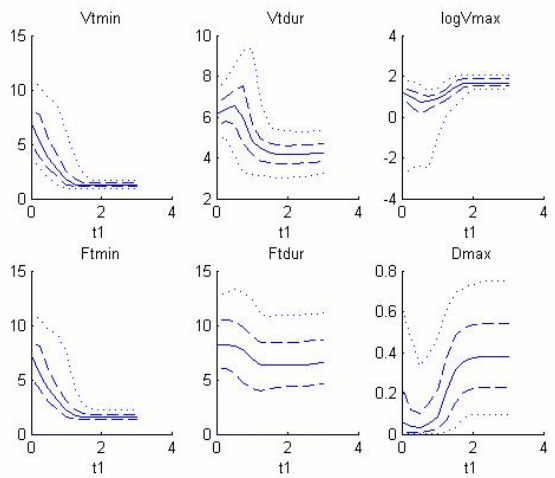
Figure 3-15. Immune response to virulent flu treated with low efficiency antiviral drug administered starting at time t1 for 7 days. a) S(0)=0 b)S(0)=0.07 c)S(0)=0.2 d)S(0)=0.4.
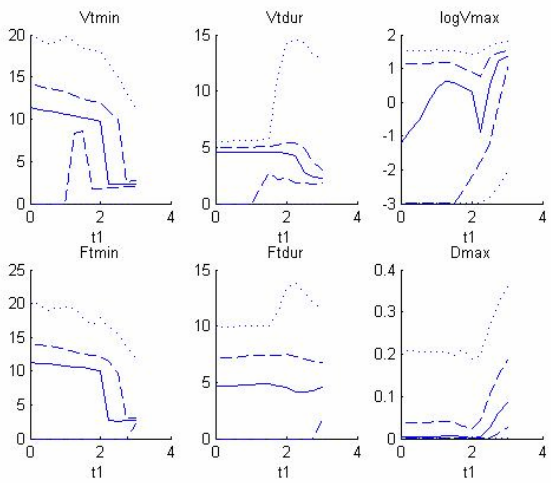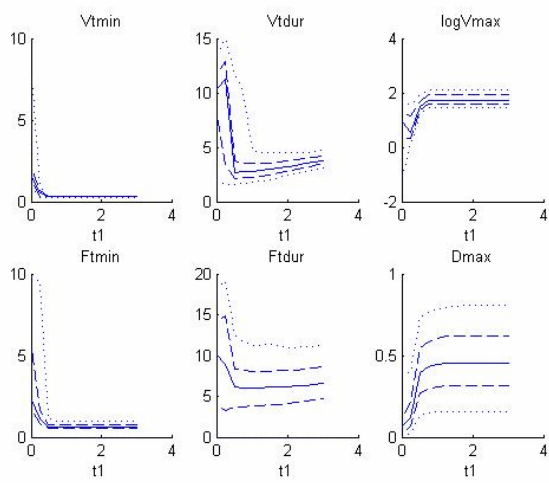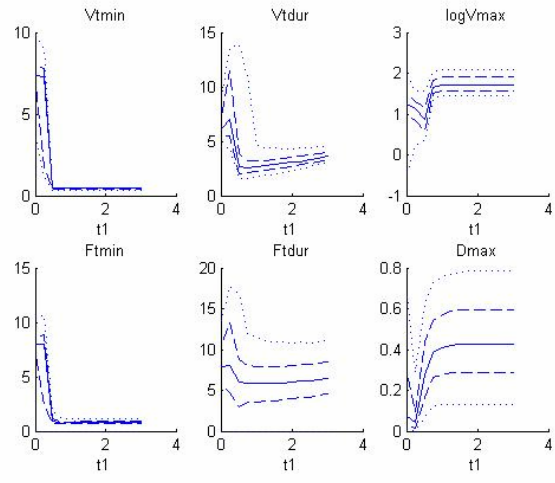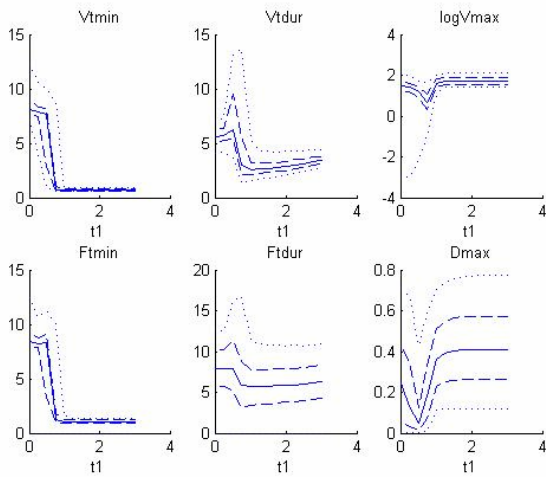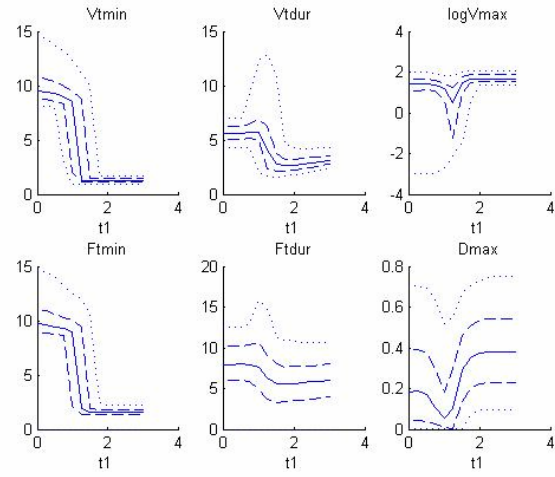
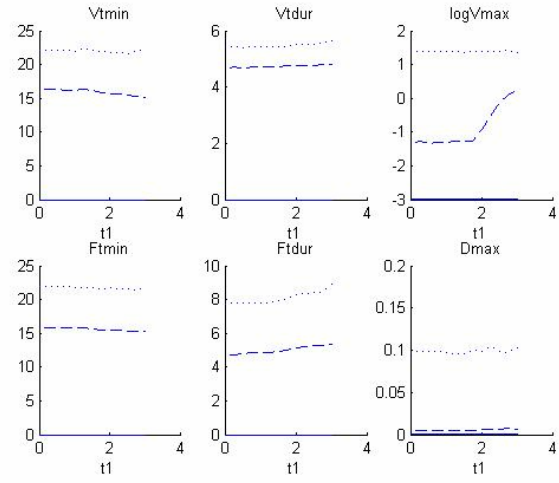**Figure 3-16. Immune response to virulent flu treated with high efficiency antiviral drug administered starting at time t1 for 7 days. a) S(0)=0 b)S(0)=0.07 c)S(0)=0.2 d)S(0)=0.4.**

individuals(S(0)=0.07), these ratios are 5% and 25% respectively. So, higher dosages actually make the case worse. Low dosage or low efficient drug given at the beginning of infection is preferable. For immune population, the effect of various dosages is similar.

3.3.3.3 Sensitivity to virulence

We investigated the impact of virulence on onset, duration, contagious period, infectiousness and severity of symptoms in cases where the low effective drug therapy and high effective drug therapy is applied.

a) Low dosage

When low dosage is chosen; the more virulent the virus, the more shortened the onset. More virulent virus causes increased transmission rates especially for vaccinated individuals or for an immune population. For naïve population virus type has no effect on making people more infectious. Duration and severity of disease is increased by virulence. For naïve population, 25% of people are becoming symptomatic caused by an infection with low virulent IAV, while 70% of them are becoming symptomatic caused by an infection with high virulent virus after the treatment. For an immunized population, everybody is likely to be cured for IAV caused by the low virulent virus. However, only half of the population is cured for infection caused by the high virulent virus.

b) High dosage

When high dosage is chosen; the more virulent the virus, the more shortened the onset. More virulent virus causes increased transmission rates. Duration and severity of disease is increased by virulence. For naïve population, 5% of people are becoming symptomatic caused by an infection with low virulent IAV, while 30% of them are becoming symptomatic caused by an infection with high virulent virus after the treatment. For an immune population, everybody is

likely to be cured for IAV caused by the low virulent virus. However, only half or less percentage of the population is cured for infection caused by the high virulent virus.

3.4   DISCUSSION

In this part, we presented an ensemble model for human immune response to the IAV infection which varies in parameter values and are ranked according to their likelihood to capture clinically available data. We extended the deterministic ODE model presented in part 1 to obtain a posteriori distribution which contains all the information on the parameter space using the information inferred from a priori knowledge. A priori information is provided by the actual data measurements and biologically reasonable ranges for parameter values (Bocharov et al., 1994; Hancioglu et al., 2007). Using the Bayesian approach, we quantified uncertainty in model predictions due to individual variability (being superspreader, immunocompressed, etc.) of the human immune response to specific virus characteristics such as virulence. This approach combines the a priori information $\theta(\alpha)$ that we have on the parameter space with the deterministic ODE model **m** to define a probability density function $\rho(\alpha)$ in M representing the a posteriori information. The distribution $\rho(\alpha)$ gives the complete solution of the inverse problem as described above and distinguishes all the information we have on the model space.

The most likely parameter values for the influenza model are determined using Metropolis algorithm as the parameters that maximize the likelihood of observing the clinical data. We incorporated parallel tempering method to improve sampling the parameter vectors. 5 replicas of the system are simulated at a series of temperatures. Configurations of 5 replicas at

83

adjacent temperatures are exchanged partially by swapping. Swapping allows the lower temperature systems to escape from one local minima of parameter space where they could easily stuck to sample larger volumes of the parameter space enhancing the sampling of local minima over M.

For many phenomena in the nature, repeated observations under a specified set of conditions invariably leads to the same outcome. Scientists can analyze these phenomena with deterministic approach, by modeling it with the tools of ODE or PDE Theory. However, there are other phenomena whose repeated observations under a specified set of conditions do not always lead to the same outcome. In our case, we consider human immune response to IAV infection as the latter due to lack of data & information on time series of model variables, individual specific parameters representing reaction rates of several biological processes within the host and unknown virus specific characteristics (mild versus virulent virus). At first sight, it may look like impossible to make any worthwhile statements considering such random phenomena, but this is not so. Our results illustrate the point that the nondeterministic biological phenomena (immune response in our case) exhibit a statistical regularity that makes it subject to study. In the deterministic approach, one set of parameter set is found for the ODE system representing the disease dynamics through optimization schemes associated with the *best model* fitting the clinical data. However, as we pointed out above, this parameter set is a biased estimator of the model space due to unpredictable nature of future influenza virus strains and the individual variability of response. In the ensemble model method we presented in this part instead, we take into account all uncertainty in parameters as a more realistic and unbiased approach to the inverse problem and still provide firm, precise assertions on clinical outcome. These results have broad implications for infectious disease epidemiology, and open challenges

for further work. Novel mathematical contribution in this thesis is the development and analysis of the influenza model and the application of ensemble modeling techniques to parameter estimation for complex biological systems.

An important issue for users of MCMC methods is to allow sampling to continue until the resulting distribution is reasonably close to the stationary distribution of interest, and therefore use the samples to estimate characteristics of this distribution. This encapsulates the issue of convergence of MCMC sampling methods. Usually, MCMC users address the convergence problem by applying diagnostic tests to the output produced by running their samplers. There are several methods that assess convergence, but all of these methods may yield misleading results depending of the nature of the problem at hand. A combination of strategies aimed at accelerating, and evaluating convergence should be used. These include monitoring autocorrelations and cross-correlations, modifying parameterizations or sampling algorithms appropriately and applying diagnostic procedures to a small number of parallel chains. However, it is not possible to conclude with certainty that a finite sample obtained through an MCMC algorithm is representative of an underlying stationary distribution *(Cowles et al., 1996).* Many statisticians rely heavily on these diagnostics for no other reason than "a weak diagnostic is better than no diagnostic at all"*(Cowles et al., 1996).*

Efforts to solve the problem of determining MCMC algorithm convergence have concentrated on two areas. The first area is theoretical in which the Markov transition kernel of the chain is analyzed to predetermine a number of iterations that will ensure convergence in total variation distance to within a specified tolerance of the stationary distribution (Polson, 1996; Rosenthal, 1996). In the trivial situation where a Markov chain has a transition kernel explicitly formulated as a matrix, the second eigenvalue provides an explicit quantization of convergence

time. The second approach is the one that most applied work based on applying the diagnostic tools to output produced by the algorithm itself.

All of the diagnostics seek to uncover bias arising from a sample that is not representative of the underlying distribution. Some of them estimate how many samples should be drawn to produce estimates with variance sufficiently small to build confidence in their accuracy. It has been found that many of the diagnostics produce results which are difficult to interpret with confidence and are potentially misleading even in the idealized settings *(Cowles et al., 1996)*. Any convergence diagnostic test should not be unilaterally relied upon and the use of several techniques to increase understanding of the target distribution is strongly recommended(Brooks et al., 1999).

The statistical analysis on the output can be categorized into two groups: Descriptive Statistics and Convergence Diagnostics. Using Descriptive Statistics tools, the modeler can compute autocorrelations, cross-correlations, and summary statistics. Histograms of the parameters and time series plots also give evidence of the convergence. High auto-correlations indicate slow mixing within a chain and, usually, slow convergence to the posterior distribution. Correlation matrix for the parameters in each chain is a good tool, too. High correlation among parameters leads to slow convergence. In order to reduce the amount of cross-correlation, clever reparametrization is needed. Summary statistics include the sample means and standard deviations.

The most commonly used methods used to assess the convergence of MCMC output are discussed below:

1) Brooks, Gelman & Rubin Convergence Diagnostic:

The Brooks, Gelman and Rubin convergence diagnostic is appropriate for the analysis of two or more parallel chains, each with different starting values which are overdispersed with

respect to the target distribution. Several methods for generating starting values for the MCMC samplers have been proposed (Gelman and Rubin, 1992). Since we used the same starting point for the chains, this diagnostic test is not appropriate to us.

2) Geweke Convergence Diagnostic:

The Geweke Convergence Diagnostic is appropriate for the analysis of individual chains such as ours when convergence of the mean of some function of the sampled parameters is of interest. The chain is divided into two windows. This method produces a Z statistics calculated as the difference between the two means of the windows divided by the asymptotic standard error of their difference. If the chain has converged, as the number of iterations approaches infinity, the Z statistics approaches the N(0,1).

3) Heidelberg and Welch Convergence Diagnostic:

The Heidelberg and Welch Convergence Diagnostic is appropriate for the analysis of individual chains. Heidelberg and Welch's stationarity test based on Brownian bridge theory and uses the Cramer-von-Mises statistic. Failure of the chain to pass this test indicates that a longer run of the MCMC sampler is needed in order to achieve convergence.

4) Raftery and Lewis Convergence Diagnostic:

The Raftery and Lewis Convergence Diagnostic is appropriate for the analysis of individual chains such as ours. The diagnostic proposed by Raftery and Lewis tests for convergence to the stationary distribution and estimates the run-lenghts needed to accurately estimate quantiles of functions of the parameters. The user may specify the quantile of interest, the desired degree of accuracy in estimating this quantile, and the probability of attaining the indicated degree of accuracy. It lists the total number of iterations needed for each parameter, the number of initial iterations to discard as the burn-in set, and the thinning interval to be used. If

the dependence factors measured is greater than 5.0 then it indicates convergence failure and a need to reparameterize the model (Raftery and Lewis, 1992).

The convergence diagnostics of Gelman and Rubin(Gelman et al., 1992) and of Raftery and Lewis (Raftery et al., 1992) are the most popular in the statistical community. Methods by Garren and Smith(1993), (Geweke, 1992), (Johnson, 1994), Liu, Liu and Rubin(Liu et al., 1992; Roberts, 1992),Yu(1994), Yu and Mykland(1994), and Zellner and Min(Zellner et al., 1995) have also been proposed. The measure of convergence in this thesis is graphical (as in some of the above methods). A more thorough and deeper analysis of convergence relevant to the specific problem discussed in this thesis may be done as a future extension of this project. As pointed out in *Cowles et al.,* many of the MCMC diagnostics proposed in the statistical literature are fairly difficult to implement, requiring problem-specific coding and some analytic work. They may not succeed at detecting the sort of convergence failure they were designed to identify even in low-dimensional idealized problems far simpler than our high-dimensional one. So, further research needs to be done by statisticians in both applied and theoretical aspects of these algorithms. There are several Bayesian output analysis programs which can be used for our sampling and they are mostly publicly available.

Despite claims in the literature somehow to the effect that some methods may be significantly superior in assessing convergence, it appears that a proper balance between implementation time and collective reliability of a number of methods should be considered, given that reliability of a single method may be highly dependent of the specific problem at hand (Brooks et al., 1999).

The ensemble model predicts that 0.6% of the population becomes superspreaders in seasonal flu outbreaks. Public health authorities should target this small proportion of the

population in order to control the epidemic more efficiently. Identifying these individuals requires a better understanding of factors (host, pathogen and environmental) determining individual infectiousness and subject of further studies.

Our results also indicate that 2% of people develop chronic disease in a regular influenza outbreak. Reduction in the production of plasma cells indicates insufficient adaptive immune response to the infection causing chronic behavior, in accord with our observations in the first part (see subsection 2.5.4.5).

Antiviral drug therapy is an important control measure to prevent from the disease and to control an epidemic. Determining the optimal treatment strategy for antiviral drugs is a crucial problem affecting not only recovery of an individual but also efficiency to disease spread.

The higher the dosage or efficiency of the drug, the more the onset of disease is prolonged. This delay on onset might be as much as 3 weeks and it gives an opportunity for the host to clear the infection even before it comes to peak with another strategy such as increased immunity.

The optimal starting time of treatment is not obvious. It depends on the immune status of the host as well as virus specific characteristics. Proper vaccination or early exposure to the same subtype of the virus helps reduce the spread of disease, severity of symptoms and transmission rates. A low dosage or low efficient drug, given at the beginning of infection, is preferable for weak immune individuals for the regular (seasonal) flu epidemic. For these people, choosing higher efficiency drug treatment actually makes the case worse. For the immune population, effect of low or high dosages is similar. So, low efficiency drug is quite enough for therapy to avoid *side effects*, which is an important parameter to consider searching for optimal strategies (there is no *arbitrage,* a well known financial term meaning free lunch). For virulent viruses, the

optimal time to start treatment is neither as early as possible nor right after infection. If it starts at day 0, it would just make the transmission rates higher and symptoms more severe in an epidemic. This effect might be explained by insufficient stimulation of immune response caused by less activated *APC*s. Infected cells (*I*) are not becoming *D* as fast as in the no treatment case and infectious virus particles are not released from *I* as much as in the no treatment case. So, due to early intervention *D* and *V* levels are initially lower causing lower immune response.

Increased computational power and using multimodel ensembles in which each single model run is deterministic composed of a parameter set taken from the distribution would enhance the results we could get. This new approach to disease modeling requires more work to be done to provide fully reliable, flow dependent probabilistic predictions. Future work would include investigation of alternative treatment strategies such as combination of several drug treatments, anti HA inhibitors and various vaccine strategies to control disease spread at population level. Availability of more clinical data and computational power would enhance the derivation of the posterior probability and give more reliable and accurate results.

BIBLIOGRAPHY

Ada, G.L.,.Jones, P.D., 1986. The immune response to influenza infection. Curr. Top. Microbiol. Immunol., 128, 1-54.

Akira, S., Takeda, K., Kaisho, T., 2001. Toll-like receptors: critical proteins linking innate and acquired immunity. Nat. Immunol., 2, 675-680.

Asquith, B.,.Bangham, C.R., 2003. An introduction to lymphocyte and viral dynamics: the power and limitations of mathematical analysis. Proc. Biol. Sci., 270, 1651-1657.

Bocharov, G.A.,.Romanyukha, A.A., 1994. Mathematical model of antiviral immune response. III. Influenza A virus infection. J. Theor. Biol., 167, 323-360.

Brooks, S.P.,.Roberts, G.O., 1999. Assessing Convergence of Markov Chain Monte Carlo Algorithms. Statist. Comp., 8, 319-335.

Chow, C.C., Clermont, G., Kumar, R., Lagoa, C., Tawadrous, Z., Gallo, D., Betten, B., Bartels, J., Constantine, G., Fink, M.P., Billiar, T.R., Vodovotz, Y., 2005. The acute inflammatory response in diverse shock states. Shock, 24, 74-84.

Clermont, G., Bartels, J., Kumar, R., Constantine, G., Vodovotz, Y., Chow, C., 2004. *In silico* design of clinical trials: a method coming of age. Crit Care Med., 32, 2061-2070.

Couch, R.B.,.Kasel, J.A., 1983. Immunity to influenza in man. Annu. Rev. Microbiol., 37, 529-549.

Cowles, M.K.,.Carlin, B.P., 1996. Markov Chain Monte Carlo Convergence Diagnostics: A Comparative Review. Journal of the American Statistical Association, 91, 883-904.

Earl, D.J.,.Deem, M.W., 2005. Parallel Tempering:Theory, applications, and new perspectives. Phys. Chem. Chem. Phys., 7, 3910-3916.

Epstein, S.L., Lo, C.Y., Misplon, J.A., Bennink, J.R., 1998. Mechanism of protective immunity against influenza virus infection in mice without antibodies. J. Immunol., 160, 322-327.

Feller, W. 1970. An Introduction to Probability Theory and Its applications New York.

Gelman, A.,.Rubin, D.B., 1992. Inference from Iterative Simulation Using Multiple Sequences. Statistical Science, 7, 457-511.

Geweke, J., 1992. Evaluating the Accuracy of Sampling-Based Approches to the Calculation of Posterior Moments. Bayesian Statistics, 4, 169-193.

Gneiting, T.,.Raftery, A.E., 2005. Atmospheric science. Weather forecasting with ensemble methods. Science, 310, 248-249.

Hancioglu, B., Swigon, D., Clermont, G., 2007. A dynamical model of human immune response to influenza A virus infection. J. Theor. Biol., 246, 70-86.

Hayden, F.G., Fritz, R., Lobo, M.C., Alvord, W., Strober, W., Straus, S.E., 1998. Local and systemic cytokine responses during experimental human influenza A virus infection. Relation to symptom formation and host defense. J. Clin. Invest, 101, 643-649.

Iwasaki, T.,.Nozima, T., 1977. Defense mechanisms against primary influenza virus infection in mice. I. The roles of interferon and neutralizing antibodies and thymus dependence of interferon and antibody production. J. Immunol., 118, 256-263.

Jaqaman, K.,.Danuser, G., 2006. Linking data to models: data regression. Nat. Rev. Mol. Cell Biol., 7, 813-819.

Johansson, B.E., Bucher, D.J., Kilbourne, E.D., 1989. Purified influenza virus hemagglutinin and neuraminidase are equivalent in stimulation of antibody response but induce contrasting types of immunity to infection. J. Virol., 63, 1239-1246.

Johnson, V.E., 1994. Studying Convergence of Markov Chain Monte Carlo Algorithms. Journal of the American Statistical Association, 91, 154-166.

Joklik, W.K., 1985. Interferons., in: Fields, B.N., Knipe, R.M., Melnick, J.L., Chanok, M.S., Riozman, B., Shope, R.E. (Eds.), Virology Raven Press, New York, pp. 281-307.

Julkunen, I., Melen, K., Nyqvist, M., Pirhonen, J., Sareneva, T., Matikainen, S., 2000. Inflammatory responses in influenza A virus infection. Vaccine, 19 Suppl 1, S32-S37.

Keenan, K.P., Combs, J.W., McDowell, E.M., 1982. Regeneration of hamster tracheal epithelium after mechanical injury. I. Focal lesions: quantitative morphologic study of cell proliferation. Virchows Arch. B Cell Pathol. Incl. Mol. Pathol., 41, 193-214.

Kuiken, T., Holmes, E.C., McCauley, J., Rimmelzwaan, G.F., Williams, C.S., Grenfell, B.T., 2006. Host species barriers to influenza virus infections. Science, 312, 394-397.

Lamb R, K. R. 1996. Orthomyxoviridae:the viruses and their replication Lippincott-Raven Publishers, Philadelphia. 1353-1396.

Liew, F.Y., Russell, S.M., Appleyard, G., Brand, C.M., Beale, J., 1984. Cross-protection in mice infected with influenza A virus by the respiratory route is correlated with local IgA antibody rather than serum antibody or cytotoxic T cell reactivity. Eur. J. Immunol., 14, 350-356.

Liu, C., Liu, J., Rubin, D.B., 1992. A Variational Control Variable for Assessing the Convergence of the Gibbs Sampler. Proceedings of the American Statistical Association 74-78.

Lloyd-Smith, J.O., Schreiber, S.J., Kopp, P.E., Getz, W.M., 2005. Superspreading and the effect of individual variation on disease emergence. Nature, 438, 355-359.

Marchuk, G.I.,.Berbentsova, E.P., 1986. [Results using a quantitative method for evaluating the severity and dynamics of acute pneumonia, chronic bronchitis and bronchial asthma]. Ter. Arkh., 58, 63-70.

Marchuk, G.I., Petrov, R.V., Romanyukha, A.A., Bocharov, G.A., 1991. Mathematical model of antiviral immune response. I. Data analysis, generalized picture construction and parameters evaluation for hepatitis B. J. Theor. Biol., 151, 1-40.

Meltzer, M.I., Cox, N.J., Fukuda, K., 1999. The economic impact of pandemic influenza in the United States: priorities for intervention. Emerg. Infect. Dis., 5, 659-671.

Mohler, L., Flockerzi, D., Sann, H., Reichl, U., 2005. Mathematical model of influenza A virus production in large-scale microcarrier culture. Biotechnol. Bioeng., 90, 46-58.

Murphy, B.R.,.Clements, M.L., 1989. The systemic and mucosal immune response of humans to influenza A virus. Curr. Top. Microbiol. Immunol., 146, 107-116.

Neumann, A.U., Lam, N.P., Dahari, H., Gretch, D.R., Wiley, T.E., Layden, T.J., Perelson, A.S., 1998. Hepatitis C viral dynamics in vivo and the antiviral efficacy of interferon-alpha therapy. Science, 282, 103-107.

Nguyen, H.H., Boyaka, P.N., Moldoveanu, Z., Novak, M.J., Kiyono, H., McGhee, J.R., Mestecky, J., 1998. Influenza virus-infected epithelial cells present viral antigens to antigen-specific CD8+ cytotoxic T lymphocytes. J. Virol., 72, 4534-4536.

Nicholson K.G, Webster A.G, and Hay A.J. 1998. Textbook of influenza Oxford: Blackwell Science.

Nowak, M. A. and R. and May. 2000. Virus Dynamics: The Mathematical Foundations of Immunology and Virology Oxford University Press.

Nowak, M.A.,.Bangham, C.R., 1996. Population dynamics of immune responses to persistent viruses. Science, 272, 74-79.

Perelson, A.S., 2002. Modelling viral and immune system dynamics. Nat. Rev. Immunol., 2, 28-36.

Perelson, A.S., Kirschner, D.E., De, B.R., 1993. Dynamics of HIV infection of CD4+ T cells. Math. Biosci., 114, 81-125.

Perelson, A.S., Neumann, A.U., Markowitz, M., Leonard, J.M., Ho, D.D., 1996. HIV-1 dynamics in vivo: virion clearance rate, infected cell life-span, and viral generation time. Science, 271, 1582-1586.

Polson, N.G., 1996. Convergence of Markov Chain Monte Carlo Algorithms. Bayesian Statistics.

Price, G.E., Gaszewska-Mastarlarz, A., Moskophidis, D., 2000. The role of alpha/beta and gamma interferons in development of immunity to influenza A virus in mice. J. Virol., 74, 3996-4003.

Raftery, A.E.,.Lewis, S., 1992. How Many Iterations in the Gibbs Sampler. Bayesian Statistics, 4, 763-773.

Roberts, G.O., 1992. Convergence Diagnostics of the Gibbs Sampler. Bayesian Statistics, 4, 775-782.

Ronni, T., Sareneva, T., Pirhonen, J., Julkunen, I., 1995. Activation of IFN-alpha, IFN-gamma, MxA, and IFN regulatory factor 1 genes in influenza A virus-infected human peripheral blood mononuclear cells. J. Immunol., 154, 2764-2774.

Rosenthal, J.S., 1996. Rates of Convergence for Data Augmentation. Annals of Applied Probability, 3, 819-839.

Sareneva, T., Matikainen, S., Kurimoto, M., Julkunen, I., 1998. Influenza A virus-induced IFN-alpha/beta and IL-18 synergistically enhance IFN-gamma gene expression in human T cells. J. Immunol., 160, 6032-6038.

Scherle, P.A., Palladino, G., Gerhard, W., 1992. Mice can recover from pulmonary influenza virus infection in the absence of class I-restricted cytotoxic T cells. J. Immunol., 148, 212-217.

Shinya, K., Ebina, M., Yamada, S., Ono, M., Kasai, N., Kawaoka, Y., 2006. Avian flu: influenza virus receptors in the human airway. Nature, 440, 435-436.

Smith, D.J., Forrest, S., Ackley, D.H., Perelson, A.S., 1999. Variable efficacy of repeated annual influenza vaccination. Proc. Natl. Acad. Sci. U. S. A, 96, 14001-14006.

Stark, G.R., Kerr, I.M., Williams, B.R., Silverman, R.H., Schreiber, R.D., 1998. How cells respond to interferons. Annu. Rev. Biochem., 67, 227-264.

Swendsen, R.H.,.Wang, J.S., 1986. Replica Monte Carlo simulation of spin glasses. Phys. Rev. Lett., 57, 2607-2609.

Tamura, S., Iwasaki, T., Thompson, A.H., Asanuma, H., Chen, Z., Suzuki, Y., Aizawa, C., Kurata, T., 1998. Antibody-forming cells in the nasal-associated lymphoid tissue during primary influenza virus infection. J. Gen. Virol., 79 (Pt 2), 291-299.

Tamura, S.,.Kurata, T., 2004. Defense mechanisms against influenza virus infection in the respiratory tract mucosa. Jpn. J. Infect. Dis., 57, 236-247.

Tamura, S., Tanimoto, T., Kurata, T., 2005. Mechanisms of broad cross-protection provided by influenza virus infection and their application to vaccines. Jpn. J. Infect. Dis., 58, 195-207.

Taubenberger, J.K.,.Morens, D.M., 2006. 1918 Influenza: the mother of all pandemics. Emerg. Infect. Dis., 12, 15-22.

Tulp, A., Verwoerd, D., Dobberstein, B., Ploegh, H.L., Pieters, J., 1994. Isolation and characterization of the intracellular MHC class II compartment. Nature, 369, 120-126.

Webster, R.G., Peiris, M., Chen, H., Guan, Y., 2006. H5N1 outbreaks and enzootic influenza. Emerg. Infect. Dis., 12, 3-8.

Wiggins, R.A., 1969. Monte Carlo Inversion of body wave observations. Journal of Geophysical Research, 74, 3171-3181.

Wiggins, R.A., 1972. The general linear inverse problem:Implication of surface waves and free oscillations for Earth structure. Rev. Geophysics, 10, 251-285.

Wohlfart, C., 1988. Neutralization of adenoviruses: kinetics, stoichiometry, and mechanisms. J. Virol., 62, 2321-2328.

Woolhouse, M.E., Dye, C., Etard, J.F., Smith, T., Charlwood, J.D., Garnett, G.P., Hagan, P., Hii, J.L., Ndhlovu, P.D., Quinnell, R.J., Watts, C.H., Chandiwana, S.K., Anderson, R.M., 1997. Heterogeneities in the transmission of infectious agents: implications for the design of control programs. Proc. Natl. Acad. Sci. U. S. A, 94, 338-342.

Wyde, P.R., Wilson, M.R., Cate, T.R., 1982. Interferon production by leukocytes infiltrating the lungs of mice during primary influenza virus infection. Infect. Immun., 38, 1249-1255.

Yetter, R.A., Lehrer, S., Ramphal, R., Small, P.A., Jr., 1980. Outcome of influenza infection: effect of site of initial infection and heterotypic immunity. Infect. Immun., 29, 654-662.

Yewdell, J.W., Bennink, J.R., Smith, G.L., Moss, B., 1985. Influenza A virus nucleoprotein is a major target antigen for cross-reactive anti-influenza A virus cytotoxic T lymphocytes. Proc. Natl. Acad. Sci. U. S. A, 82, 1785-1789.

Yoshikawa, T., Matsuo, K., Matsuo, K., Suzuki, Y., Nomoto, A., Tamura, S., Kurata, T., Sata, T., 2004. Total viral genome copies and virus-Ig complexes after infection with influenza virus in the nasal secretions of immunized mice. J. Gen. Virol., 85, 2339-2346.

Zdanov, V.M.,.Bukrinskaja, A.G., 1969. Myxoviruses Reproduction. Medicina(in Russian).

Zellner, A.,.Min, C., 1995. Gibbs Sampler Convergence Criteria. Journal of the American Statistical Association, 90, 921-927.